Decadal reanalysis of biogeochemical indicators and fluxes in the North West European shelf-sea ecosystem

S. Ciavatta[1,2], S. Kay[1], S. Saux-Picart [1,3], M. Butenschön[1], and J. I. Allen[1,2]

[1] Plymouth Marine Laboratory, PL1 3DH Plymouth, UK

[2] National Centre for Earth Observation, Plymouth Marine Laboratory, UK

[3] Météo France, Centre de Météorologie Spatiale, 22300 Lannion, France

Corresponding author: Stefano Ciavatta (s.ciavatta@pml.ac.uk)

Key Points:

- The reanalysis dataset is skilled in estimating indicators that are relevant for marine policy.
- Large areas of shelf bottom waters are oxygen deficient at a high confidence level.
- The shelf-sea ecosystem is a net sink of atmospheric carbon dioxide (CO_2).

Abstract

In this paper we present the first decadal reanalysis simulation of the biogeochemistry of the North West European shelf, along with a full evaluation of its skill and value. An error-characterized satellite product for chlorophyll was assimilated into a physical-biogeochemical model of the North East Atlantic, applying a localized Ensemble Kalman filter. The results showed that the reanalysis improved the model predictions of assimilated chlorophyll in 60% of the study region. Model validation metrics showed that the reanalysis had skill in matching a large dataset of in situ observations for ten ecosystem variables. Spearman rank correlations were significant and higher than 0.7 for physical-chemical variables (temperature, salinity, oxygen), ~0.6 for chlorophyll and nutrients (phosphate, nitrate, silicate), and significant, though lower in value, for partial pressure of dissolved carbon dioxide (~0.4). The reanalysis captured the magnitude of pH and ammonia observations, but not their variability. The value of the reanalysis for assessing environmental status and variability has been exemplified in two case studies. The first shows that between 340,000-380,000 km^2 of shelf bottom waters were oxygen deficient potentially threatening bottom fishes and benthos. The second application confirmed that the shelf is a net sink of atmospheric carbon dioxide, but the total amount of uptake varies between 36-46 Tg C yr^{-1} at a 90% confidence level. These results indicate that the reanalysis output dataset can inform the management of the North West European shelf ecosystem, in relation to eutrophication, fishery, and variability of the carbon cycle.

1. Introduction

Trends and patterns of biogeochemical variables that are relevant for marine policy and ecosystem understanding can be evaluated by merging numerical models and ocean color in extended "biogeochemical reanalysis", using a consistent data assimilation algorithm [*Lahoz and Schneider*, 2014; *Gehlen et al.*, 2015]. Such algorithm corrects the model estimates towards the observations, taking account of the errors in the model and in the observations [*Kalman*, 1960]. The resulting estimates of biogeochemical variables are expected to be more realistic than the estimates obtained separately from modelling and monitoring efforts, as is well-established in environmental disciplines such as atmospheric science [*Bengtsson and Shukla*, 1988; *Trenberth and Olson*, 1988] and ocean physics modelling [*Stockdale et al.*, 1998].

In ocean biogeochemical modelling, the first (quasi)decadal biogeochemical reanalysis estimated the interannual variability of global primary production in years 1998-2004 by assimilating chlorophyll from SeaWiFS (Sea-viewing Wide Field-of-view Sensor) into the NASA Ocean Biogeochemical Model (OBM) [*Nerger and Gregg,* 2007]. A comparable variability of primary production was obtained in the reanalysis by *Gregg* [2008], who in addition described the spatial patterns of chlorophyll in the global oceans. The reanalysis by *Fontana et al.* [2013] evaluated spatial-temporal patterns of chlorophyll and nitrate in the North Atlantic Ocean in years 1998-2006, by assimilating SeaWiFS chlorophyll into a coupled physical-biogeochemical model. Reanalyses for years 1998-2012, using chlorophyll observations from SeaWiFS and MODIS and the NASA OBM, evaluated significant declining trends of chlorophyll in the Northern Hemisphere and Indian oceans [*Gregg and Rousseaux*, 2014], and

57 estimated declining trends of phytoplankton functional groups in part of the global oceans
58 [*Rousseaux and Gregg*, 2015].

59 The above works all demonstrated the value of reanalysis for open oceans, but the usefulness
60 of biogeochemical reanalysis has not been evaluated in extended simulations for shelf-sea
61 ecosystems yet. Shelf-seas are crucial to the earth system, by providing ~20% of the marine
62 primary production [*Jahnke*, 2010], ~20% of the uptake of atmospheric carbon dioxide (CO_2) by
63 the oceans [*Borges*, 2011] and over 90% of the global fish catches [*Pauly et al.*, 2002]. These
64 processes and services are impacted by interannual climate variability and changes in anthropic
65 pressures, implying trends in coastal eutrophication [*Cloern*, 2001], fluctuations of shelf uptake
66 of CO_2 [*Borges*, 2011] and expansion of poorly oxygenated shelf floor areas threatening fishes
67 and benthic communities [*Diaz and Rosenberg*, 2008; *Gilbert et al.*, 2010; *Rabalais et al.*, 2014].
68 Marine policy and research are cooperating in monitoring and modelling biogeochemical
69 variables that are indicators of the status of shelf ecosystems and that can characterize its long-
70 term variability, such as chlorophyll concentration, dissolved oxygen, partial pressure of CO_2,
71 nutrient concentrations [*OSPAR*, 2013]. Such indicators have been estimated successfully in
72 previous works by assimilating ocean color into shelf-sea models; however such simulations
73 were short-termed (i.e. one-year or shorter) focusing on the skill of daily to weekly operational
74 predictions [e.g., *Terruzzi et al.*, 2014; *Shulman et al.*, 2013] or on the seasonal cycle of the
75 ecosystems [e.g., *Triantafyllou et al.*, 2007; *Fontana et al.*, 2010; *Ciavatta et al.*, 2011, 2014;
76 *Mattern et al.*, 2013; *Hu et al.*, 2012; *Xiao and Friedrichs*, 2014], leaving the reanalysis of the
77 interannual variability of shelf-sea biogeochemistry unexplored.

78 The overall aim of this work was to provide the first decadal reanalysis of the
79 biogeochemistry of the North West European shelf sea. The specific objectives of this paper are:

80 i) to evaluate the skill and confidence of the reanalysis; and ii) to exemplify the value of the
81 reanalysis dataset to assess the status and interannual changes of the shelf ecosystem. With this
82 last broad objective in mind, we present two case studies assessing: a) The vulnerability of the
83 bottom waters of the shelf to oxygen deficiency; and b) The interannual variability of the uptake
84 of atmospheric CO_2 by the shelf-sea ecosystem.

85 To achieve these aim and objectives, we assimilated an error-characterized ocean color
86 product for chlorophyll [*Brewin et al.*, 2015; *Sathyendranath et al.*, 2016] into an ecosystem
87 model of the North East Atlantic [*Wakelin et al.*, 2012], upgraded to the state-of-the-art version
88 of the European Regional Seas Ecosystem Model (ERSEM) [*Butenschön et al.*, 2015] and
89 integrated into the Ensemble Kalman filter [*Evensen*, 1994; *Ciavatta et al.*, 2011]. This
90 assimilation system was applied in the reanalysis of the biogeochemistry of the North West
91 European (NWE) shelf in the years 1998-2009. The reanalysis output dataset was first skill-
92 evaluated using ocean color data and in situ observations of ten physical and biogeochemical
93 variables. The dataset was then post-processed to extract information relevant to the case studies,
94 including the confidence level of the reanalysis estimates. This latter information is a major gap
95 in most of the current modelling applications for ecosystem assessment [*Hyder et al.*, 2015;
96 *Piroddi et al.*, 2015], thus we suggest that it represents an added value of our reanalysis dataset
97 for its possible application in marine policy.

98 The paper is structured as follows. Section 2 describes the ecosystem model, the set-up of the
99 assimilation algorithm, the data, and the metrics applied for skill evaluation. In Section 3, the
100 results are presented and discussed. The skill of the reanalysis dataset is first evaluated with
101 respect to the assimilated ocean color data (Section 3.1), and then using an in situ dataset which

was not part of the assimilation (Section 3.2). The two case studies are presented in sections 3.3 and 3.4 and concluding remarks and future applications are pointed out in Section 4.

2 Material and Methods

2.1 The ecosystem model of the North East Atlantic

The ecosystem dynamics of the North East Atlantic, including the North West European shelf, (Figure 1) are described by a three-dimensional physical-biogeochemical model [*Wakelin et al.*, 2012; *Artioli et al.*, 2012; *Artioli et al.*, 2014].

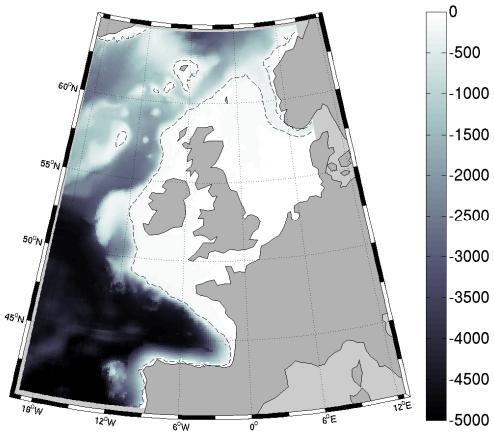

Figure 1. The North East Atlantic region represented in the model domain. The dashed line represents the 200 m isobath delimiting the shelf region for convention.

The model consists of three on-line coupled sub-models (see Figure 2): the Proudman Oceanographic Laboratory Coastal Ocean Modelling System (POLCOMS) [*Holt and James*, 2001], which describes the hydrodynamics and provides the physical forcing to the pelagic biogeochemical sub-model, namely the European Regional Seas Ecosystem Model (ERSEM)

[*Baretta et al.*, 1995; *Butenschön et al.*, 2015]. The third sub-model is the ERSEM benthic biogeochemical model [*Blackford*, 1997; *Butenschön et al.*, 2015]. The sub-models are coupled at the same temporal and spatial resolution as the physical model, to capture the effects of the three-dimensional hydrodynamics on the biogeochemical cycles [*Holt et al.*, 2004].The grid of the model spatial domain has horizontal resolution of 1/6° in longitude and 1/9° in latitude, approximating to ~12 km at the latitude of the study region, and it has 42 s-coordinate levels in the vertical [*Wakelin et al.*, 2012].

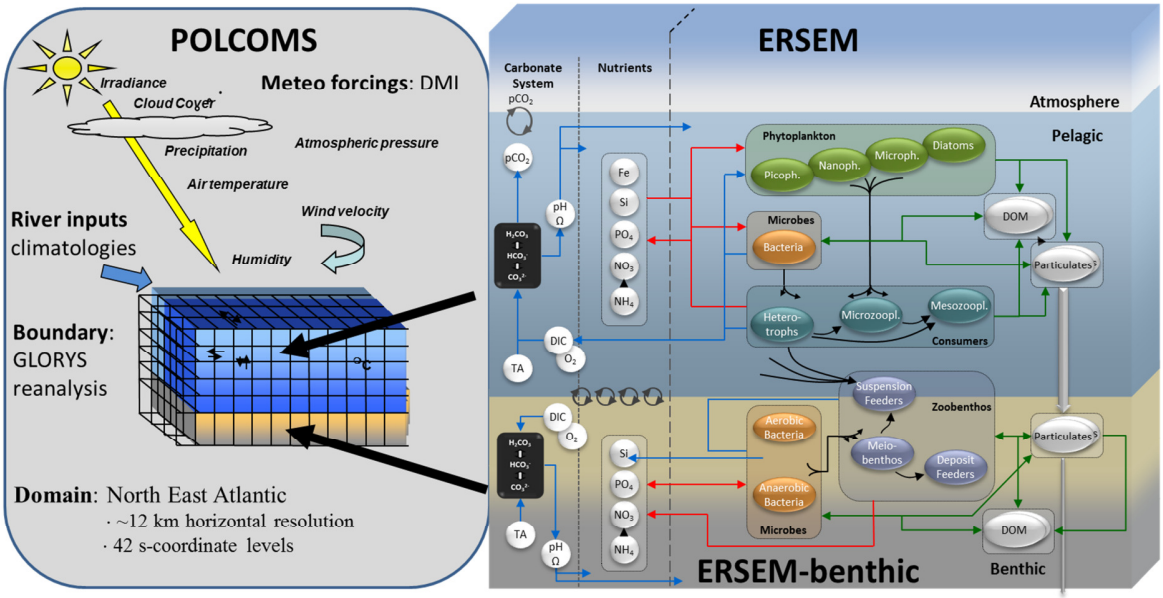

Figure 2 Schematic of the ecosystem model coupling the physical sub-model POLCOMS and the pelagic and benthic biogeochemical sub-models of ERSEM.

131 2.1.1 The physical sub-model: POLCOMS

132

133 The physical model POLCOMS [*Holt and James*, 2001] is a three-dimensional baroclinic,
134 finite-difference, primitive equation model formulated in spherical-polar coordinates on an
135 Arakawa B-grid. Both temperature and salinity are treated as prognostic variables. The model
136 includes: an advection scheme with stability and conservation properties [*James*, 1996]; a
137 vertical turbulence model (GOTM) [*Burchard et al.*, 1999]; and calculation of horizontal
138 pressure gradients.

139

140 2.1.2 The pelagic biogeochemical sub-model: ERSEM

141

142 The biogeochemical dynamics are described by the European Regional Seas Ecosystem
143 model (ERSEM) [*Baretta et al.*, 1995], using its state-of-the-art version presented in *Butenschön*
144 *et al.* [2015], and applying a configuration with 51 pelagic variables. ERSEM uses a functional
145 type approach to model the dynamics of the low trophic levels of the ecosystem. Primary
146 producers are split into four phytoplankton functional types (PFTs), including three size based
147 types (picophytoplankton, nanophytoplankon, microphytoplankton), plus diatoms as silicate
148 users. Each of these PFTs is defined in terms of its content of chlorophyll, carbon, nitrogen,
149 phosphate, and (for diatoms only) silicate. Three functional types of zooplankton
150 (mesozooplankton, microzooplankton, and heterotrophic nanoflagellates) prey on the PFTs,
151 bacteria and particulate organic matter as a function of their size. One bacterial functional type
152 drives the microbial loop, the production and recycling of dissolved organic matter in labile,
153 semi-labile and recalcitrant forms, and it drives the regeneration of inorganic nutrients in the

154 water column [*Polimene et al.*, 2006; *Hansell*, 2013]. In the functional types, the stoichiometric
155 ratios of nutrients-to-carbon and chlorophyll-to-carbon (in the PFTs) vary dynamically [*Geider*
156 *et al.*, 1997; *Baretta-Bekker et al.*, 1997]. The model includes the dynamics of five inorganic
157 dissolved nutrients (carbon, nitrate, ammonia, phosphate and silicate), and dissolved oxygen. The
158 model configuration applied here includes a carbonate system module, which regulates air-sea
159 flux of carbon dioxide, as well as the description of calcite, including its deposition at the sea
160 floor [*Artioli et al.*, 2012; *Butenschön et al.*, 2015].

161 Numerous works demonstrate the skill of ERSEM in representing marine ecosystem
162 processes and reproducing ocean observations. Model validations have used univariate and
163 multivariate analysis [e.g. *Allen and Sommerfield*, 2009; *Saux-Picart et al.* 2012, *de Mora et al.*,
164 2013, 2016] in model applications ranging from zero-dimensional process studies [e.g. *Pinna et*
165 *al.*, 2015] to global simulations [*Kwiatkowski et al.*, 2014, *de Mora et al.*, 2013]. In particular,
166 the state-of-art version applied in this work was flexible and skilled in simulating multiannual
167 time series of nutrients, chlorophyll, oxygen, particulate organic and dissolved inorganic carbon,
168 as well as reproducing emerging properties (phytoplankton stoichiometry and average
169 community structure) observed in three contrasting sites in coastal, shelf and open ocean
170 [*Butenschon et al.*, 2015, *de Mora et al.* 2016]. However, the model can have low skill in
171 representing observed phytoplankton successions (in particular blooms of dinoflagellates) in
172 large-scale shelf-sea applications, due to limitations in the parameterization of the PFTs
173 [*Ciavatta et al.*, 2011].

174

175

176 2.1.3 The ERSEM benthic sub-model

177

178 The benthic sub-model is the ERSEM benthic model [*Blackford*, 1997], as described in
179 *Butenschön et al.* [2015]. In the configuration applied here, the sub-model includes 35
180 biogeochemical variables, subdivided into seven living functional groups (including zoobenthos,
181 aerobic and anaerobic bacteria), along with particulate matter and dissolved organic and
182 inorganic nutrients. The fluxes at the sediment-water interface are determined by sedimentation
183 and diffusion of inorganic material across the seabed.

184

185 2.1.4 Boundary conditions and atmospheric forcing

186

187 The oceanic conditions at the open boundaries of the ecosystem model (temperature, salinity,
188 currents and sea surface elevation) were extracted for the years 1998-2009 from the GLORYS
189 reanalysis product provided within the EC FP7 project MyOcean [*Ferry et al.*, 2012]. The
190 corresponding conditions for dissolved nutrients and oxygen were extracted from the 2005
191 World Ocean Atlas climatology [*Garcia et al.*, 2006a; 2006b], and for dissolved inorganic
192 carbon (DIC) from the database GLODAP [*Key et al.*, 2004].

193 The model is forced by daily climatological discharges of fresh-water and dissolved nutrients
194 from 250 rivers. Data of water discharge were taken from the Global River Discharge Data Base
195 [*Vörösmarty et al.*, 1996], and from data prepared by the UK Centre for Ecology and Hydrology.
196 River nutrient loadings match those used by *Lenhart et al.* [2010], with raw data for the UK,
197 Northern Ireland, Ireland, France, Norway, Denmark and the Baltic processed by the UK Centre
198 for Environment Fisheries and Aquaculture Science, and raw data for Germany and the

199 Netherlands derived from *Pätsch and Lenhart* [2004]. In addition, Baltic inflow was represented
200 as river-inflow [*Wakelin et al.*, 2012]. Atmospheric input of nutrients was derived from the
201 European Monitoring and Evaluation Programme [*Tørseth et al.*, 2012].

202 The atmospheric forcing (three-hourly solar irradiation, air temperature, wind velocity,
203 precipitation, humidity, pressure and cloud cover), was obtained from a regional climate hindcast
204 (years 1989-2009, spatial resolution of 12 km) performed by the Danish Climate Centre, using
205 the regional Climate model HIRHAM5 [*Christensen et al.*, 2006], driven by ERA-interim global
206 reanalysis [*Dee et al.*, 2011].

207

208 2.2 The assimilation system

209

210 The assimilation framework uses the system described in full in *Ciavatta et al.* [2011, 2014],
211 where it was developed to assimilate ocean color in a similar POLCOMS-ERSEM model
212 configured for the English Channel. The system uses the Ensemble Kalman filter (EnKF)
213 [*Evensen*, 1994]. This is a sequential assimilation method, which starts by randomly sampling an
214 ensemble of *N* state vectors $\mathbf{x}_0^{a(l)}$ (l=1, 2, ..., N) from an initial probability density function for
215 the model variables. Each ensemble member, i.e. state vector, is propagated in time using the
216 non-linear model equations during the "forecast step", that provides the EnKF "forecasts" $\mathbf{x}_i^{f(l)}$.

217 At time *i*, the forecast state $\mathbf{x}_i^f$ and the forecast uncertainty $\mathbf{P}_i^f$ are defined from the mean
218 value and the covariance matrix of the N forecasted members. When at time *i* a vector $\mathbf{y}'_i$ of
219 observations of the model output $\mathbf{y}_i = \mathbf{H}[\mathbf{x}_i^{f(l)}]$ becomes available, the assimilation scheme
220 updates (i.e. "corrects") the forecasted states $\mathbf{x}_i^{f(l)}$, in the EnKF "analysis" step. This step scales

the forecast-to-data mismatches, by balancing the uncertainty in the model ($\mathbf{P}_i^f$) and in the observations ($\mathbf{R}_i$) and it provides the analysed ensemble $\mathbf{x}_i^{a(l)}$. This ensemble is the initial condition used to simulate a new ensemble forecast for time *i*+1, in a sequential procedure that estimates the evolution of the model variables over the time window spanned by the assimilated observations.

Our assimilation system uses the *Evensen* [2003] version of the EnKF, which includes localization of the analysis and perturbation of the assimilated observations [see also *Natvik and Evensen*, 2003; *Hu et al.*, 2012; *Storto et al.*, 2013]. Observations and model states are log-transformed prior to the analysis, to guarantee positivity of the solutions [*Janjic et al., 2014*], as in the applications by *Torres et al.*, [2006], *Nerger and Gregg* [2008], *Ciavatta et al.* [2011, 2014].

Importantly, the ensemble method can provide estimates of the uncertainty of the reanalysis product, derived from the dispersion of the ensemble members around their central value (i.e. the median). In particular, we used ranked values of the one-hundred ensemble members (minimum, 5^{th}, 95^{th} and maximum ensemble value) to define the confidence levels of the reanalysis estimates (1%, 5%, 95% and 100% confidence, respectively).

2.2.1 Set-up of the assimilation scheme

Following *Ciavatta et al.* [2011], we used the EnKF with an ensemble size of *N*=100 members. To keep the analysis affordable computationally, the analysed state vector had to include a maximum of forty-four out of the fifty-one biogeochemical state variables. The remaining seven variables were updated through the model equation during the simulation

runtime ("forecast" step) and were selected among those more likely to create instabilities in the long-term reanalysis on the base of previous findings (silicate in dissolved and medium and large particulate forms [*Ciavatta et al.*, 2011]), and of assimilation tests within this study (semi-labile dissolved organic carbon, dissolved oxygen, alkalinity and calcite). The radius of the localized analysis was set spatially variable as a function of the bathymetry [*Ciavatta et al.*, 2011]. In particular, we increased the "resolution" of the analysis from oceanic towards coastal waters, by setting a radius of 100 km for grid points where the bathymetry is deeper than 2000 m (i.e. in 35% of the cells of the model grid), 50 km for bathymetry between 50 – 2000 m (51% of the grid), and 25 km for bathymetry shallower than 50 m (14% of the grid).

Model error is accounted for by random perturbations of the model forcing, namely the surface solar irradiance, thus inducing fluctuations in the underwater light field that drives photosynthesis [*Torres et al.*, 2006; see *Natvik and Evensen*, 2003 and *Simon and Bertino*, 2009 for comparable approaches]. A Gaussian perturbation with standard deviation equal to 20% of the irradiance value is added during the model forecast step. Furthermore, at the first assimilation step of each year, model error is added to all the variables undergoing the analysis, as white noise drawn from a distribution of pseudo-random fields with error equal to 10% of the value of the variables. The error is lowered to 1% for those variables that have relatively high average values (DIC, ammonia, small particulate matter), to avoid divergences in the concentrations of the largest pool in the model [*Ciavatta et al.*, 2011].

The ensemble was initialized by perturbing the output of a hindcast model simulation that started in January 1991 after a five-year spin-up. The hindcast states for September 1997 were perturbed by using Gaussian pseudo-random fields with error equal to 30% of the value of the variables. These perturbed states were used to start the assimilation from the first data available

267 in the ocean color time series. Results of the reanalysis and of the simulation without
268 assimilation, namely the "reference" run, are presented for January 1998-December 2009.
269 The reanalysis simulation was run on the UK NERC High Performance Computing facility
270 "ARCHER", using 7200 CPUs and ~9 Mega Allocation Units (MAUs).
271

272 2.3 Data

273

274 The data of remotely sensed concentration of surface chlorophyll used in the assimilation
275 (Figure 3) were provided by the Ocean Colour - Climate Change Initiative project of the
276 European Space Agency (ESA's OC_CCI product, Version 2.0, [*Brewin et al.*, 2015; *Grant et*
277 *al.*, 2015; *Sathyendranath et al.*, 2016]). This product was created by merging satellite data from
278 sensors MERIS, MODIS and SeaWiFS, after shifting the wavelength bands and correcting the
279 bias between the sensors. It consists of a global daily level 3 binned dataset provided on a
280 sinusoidal grid at 4 km resolution. It was downloaded via FTP from http://www.oceancolor.org.
281 As described in Appendix 1, here the dataset was projected onto the ~12 km model grid, and
282 daily values were merged into five-day composites centered on the last day of each month in the
283 years 1998-2009. Importantly, in the assimilation scheme we made use of per-pixel error
284 statistics estimated by OC_CCI through the analysis of match-ups between in situ data and ocean
285 color [*Sathyendranath and Jackson*, 2015]. In particular, we computed and assimilated un-biased
286 values of chlorophyll observations, and we defined the variance of their pseudo-random
287 Gaussian perturbations (Section 2.2) by processing per-pixel root-mean-square-deviations
288 provided with the OC_CCI dataset (see details in Appendix 1, equations A1.8 and A1.9).
289

290

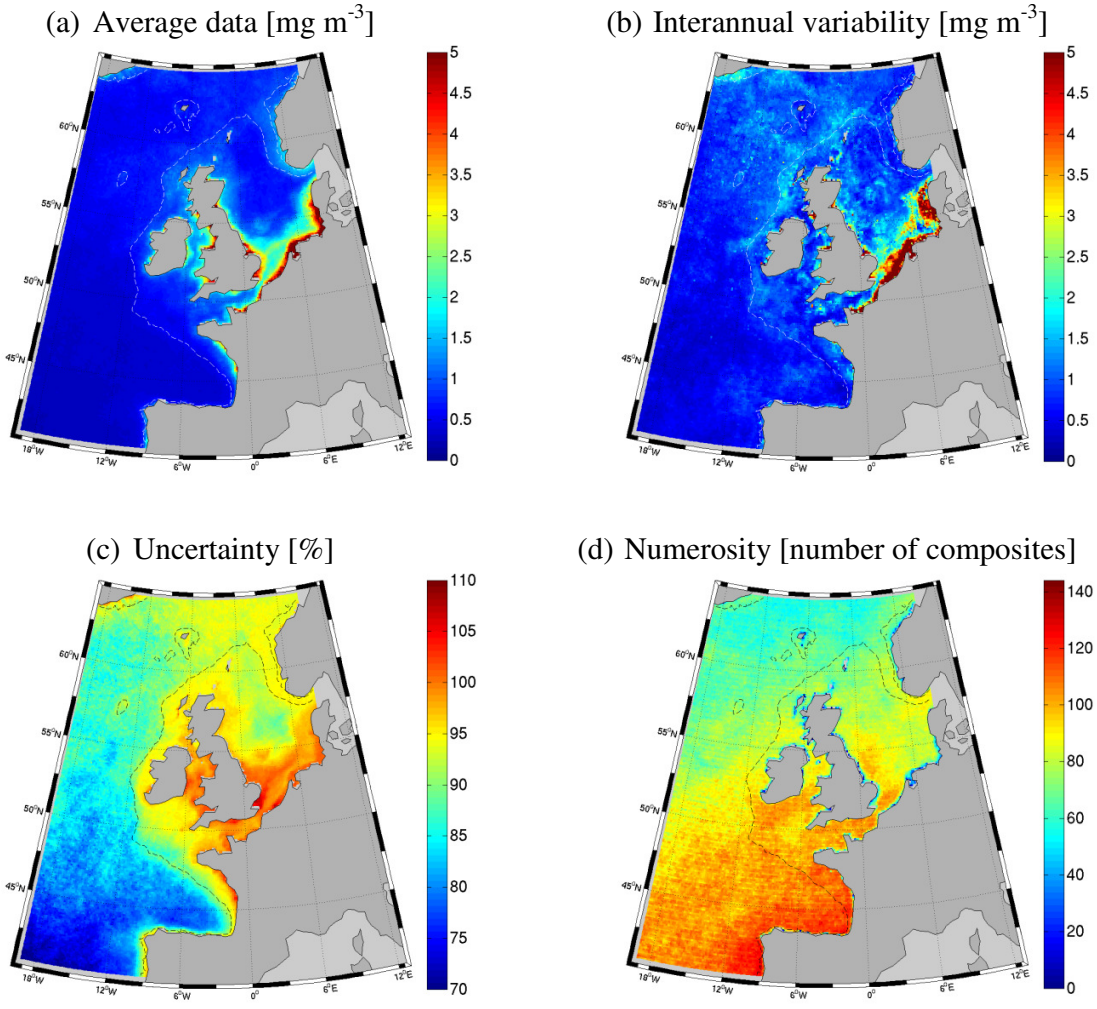

291

292 **Figure 3** Chlorophyll data from ocean color assimilated in the reanalysis; (a) average value of
293 the unbiased data in the period 1998-2009 (in concentration units, computed from y_c' in equation
294 A1.10 in Appendix 1); (b) range between the maximum and minimum yearly means; (c) average
295 value of the percentage standard deviation of the observations (computed as ratio of s_c and y_c' in
296 equations A1.10-11); (d) numerosity of the assimilated composites at each grid cell of the model
297 domain, in the 144 month long reanalysis. The dashed line represents the 200 m isobath
298 delimiting the shelf region for convention.

299

300 The in situ data used to evaluate the reanalysis skill were measured in the North East Atlantic
301 in the years 1998-2009 and were extracted from the Ecosystem Data Online Warehouse of the
302 International Council for the Exploration of the Sea (www.ices.dk) for the following variables:
303 temperature, salinity, dissolved oxygen, chlorophyll, nitrate, ammonia, phosphate, silicate and
304 pH. Data of partial pressure of carbon dioxide (pCO_2) were derived from the Surface Ocean CO_2
305 Atlas (http://www.socat.info/).

306

307 2.4 Skill metrics

308

309 The skill of the reference and reanalysis output (y) in matching the assimilated composites of
310 chlorophyll concentrations from ocean color (y'_c, eq. A.1.10 in Appendix 1) was evaluated by
311 computing and comparing maps of the root mean square deviation (RMSD) and of the Pearson
312 correlation (ρ) between the time series of y and y'_c at each surface grid point of the model
313 domain. The RMSD between the spatial distributions of y and y'_c at each month of the reanalysis
314 were also computed. The skill of the reanalysis was evaluated for the output of both the forecast
315 and analysis steps of the assimilation algorithm (see Section 2.2 for the definition of these steps).
316 Quantitative metrics to evaluate the skill of the reanalysis in matching the in situ
317 biogeochemical data were computed using an open source tool for model validation
318 (https://github.com/bcdev/opec-tools) based on *de Mora et al.* [2013]. Daily values of the
319 variables in the reanalysis dataset (y) were matched-up point-to-point in space and time with the
320 observations (o). Parametric statistics were then computed and presented in Taylor and Target
321 diagrams that show [*Taylor*, 2001; *Jolliff et al.*, 2009]: Pearson correlation coefficient (ρ),

322 standard deviation of the output (σ) normalized by the standard deviation of the observations
323 (σ_o), bias of the output, bias=mean(y-o), normalized by σ_o, unbiased root mean square deviation
324 (RMSD') normalized by σ_o and taken with the algebraic sign of the differences between the
325 standard deviation of the output and the observations, sign(σ-σ_o). In addition, we computed
326 "robust" skill metrics that are sounder than parametric metrics when the distribution of the
327 variables is non-gaussian, because robust metrics are based on the percentiles and ranks of the
328 distributions and thus they are less affected by outliers [e.g., *Daszykowski et al.*, 2007]. Robust
329 metrics were presented in a Target diagram showing [*Butenschön et al.*, 2015]: the bias
330 computed as the median value of the reanalysis-to-observation mismatch, *bias**=median(*y-o)*,
331 normalized by the interquartile range of the observations (IQR_o); the unbiased median absolute
332 error, MAE'=median{abs[*y-o-bias**]}, normalized by IQR_o, and taken with the algebraic sign of
333 the differences between the interquartile range of the output and the observations, sign(IQR-
334 IQR_o); the Spearman rank correlation coefficient, ρ_s. The latter was used also in the case studies,
335 to compute cross-correlation among time series of variables from the reanalysis; we computed
336 also the significance level *p* that such correlation is different from zero, at a confidence level of
337 99%, that is $p<0.01$.
338

339 **3 Results and discussion**

340 3.1 Skill in matching the ocean color data

341

342 In the years 1998-2009, the distribution of chlorophyll observed in the North West European
343 shelf was characterized by sharp gradients from the coastal areas towards the oceanic waters
344 (Figure 3a), and the reanalysis matched this pattern quite closely (Figure 4).

345 Simulated concentrations were lower than satellite observations in coastal areas, however the
346 satellite observations were more uncertain in these regions compared to the open shelf (Figure
347 3c), due to re-suspended sediments and colored dissolved organic matter discharged by rivers
348 [*Sathyendranath et al.*, 2000]. In oceanic waters, the reanalysis overestimated the observed
349 chlorophyll concentrations because the model was overestimating nutrients in the boundary
350 ocean regions (see Section 3.2). In addition, in the northern oceanic waters, the skill of the
351 reanalysis was constrained by the relatively low number of data items available for assimilation
352 (Fig 3d).

353

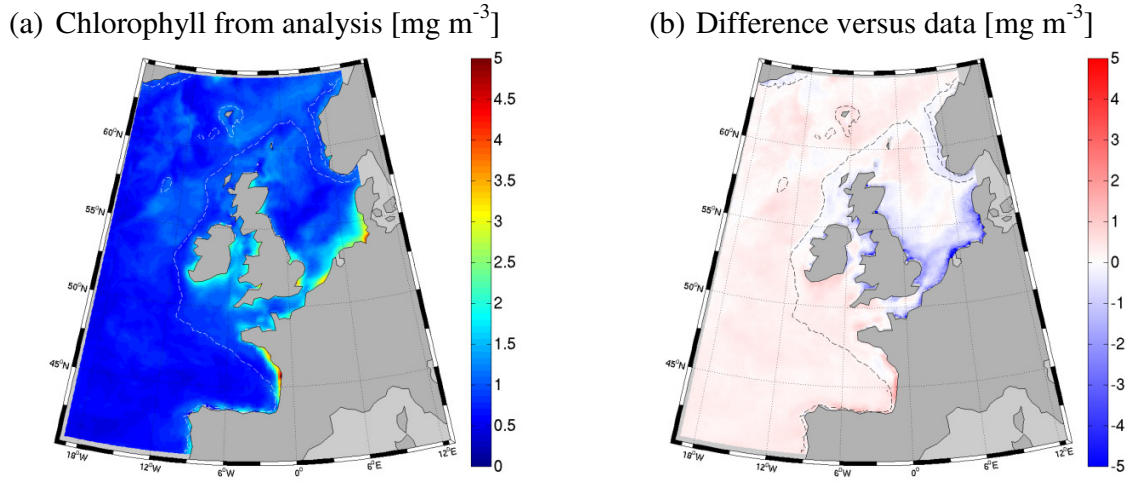

354 **Figure 4** (a) Average spatial distribution of chlorophyll concentration from the monthly
355 assimilative analyses, in years 1998-2009; and (b) difference of such distribution with respect to
356 the average value of the unbiased ocean color data shown in Figure 3a. The dashed line
357 represents the 200 m isobath delimiting the shelf region for convention.

358

The reanalysis had skill in matching the assimilated satellite observations (Figure 5). The seasonal cycles of the observations were captured by the simulation, as demonstrated by the large areas where the correlation coefficient is higher than 0.6. Some low, or even negative, correlations were computed in the northern basin where observations were sparse, and in coastal areas where observations were more uncertain, limiting the ability of assimilation to correct the model (Figs. 3c and 3d). The RMSD between reanalysis and data is comparable to the chlorophyll concentrations in large parts of the domain, when averaged over the whole period 1998-2009 (Fig 4a and 5a). Temporal mismatches between simulation and observations (e.g. misrepresented phytoplankton blooms) contributed to the high RMSD in the coastal areas.

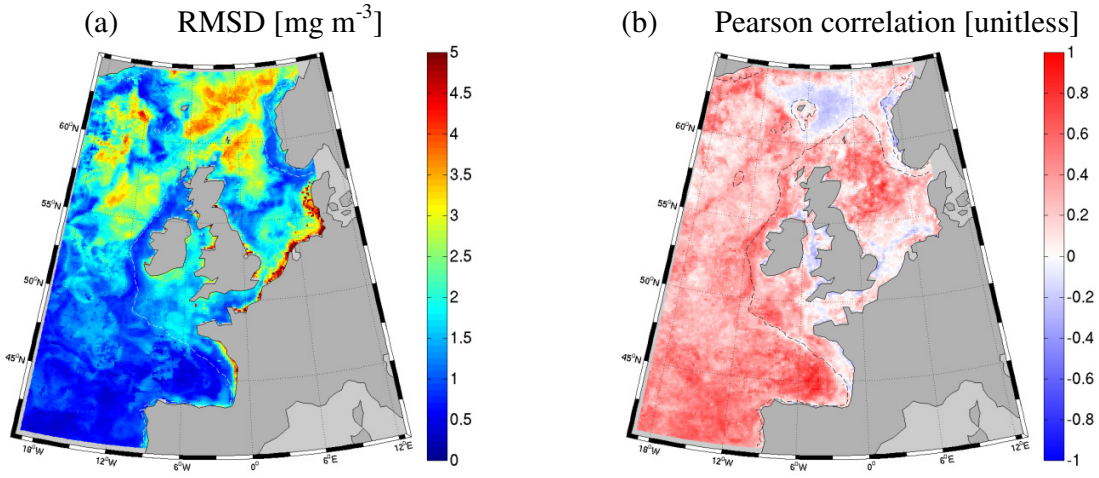

Figure 5 Skill of the reanalysis in simulating the assimilated chlorophyll data: (a) root mean square deviation (RMSD); and (b) Pearson correlation between monthly time series of simulated and observed data at each grid point of the model domain, in the period 1998-2009. The dashed line represents the 200 m isobath delimiting the shelf region for convention.

375 The reanalysis product has a higher skill in matching the ocean color data than the output of
376 the model without data assimilation, i.e. the model reference run. Importantly, this holds for the
377 one-month "forecasts" of the assimilation run (i.e. the output before the assimilation step), as
378 well as for the "analysis" (i.e. the output after the assimilation step) (Figure 6). Both the analyses
379 and forecasts decreased the RMSD of the reference run by at least 1% in ~60% of the basin
380 (Figs. 6a and 6c). The already high reference correlations were not changed markedly by the
381 forecasts and analyses, since in both cases changes were smaller than 0.01 in ~60% of the basin
382 (Figs 6b and 6d). Improvements of the reference simulation were higher in magnitude for the
383 analysis than for the forecasts, and the analysis decreased the reference RMSD up to 20% (Fig.
384 6a). In general, improvements were less evident in the coastal areas and in the northern basin, but
385 here the assimilated data had higher errors and were less numerous, respectively, as mentioned
386 above.
387

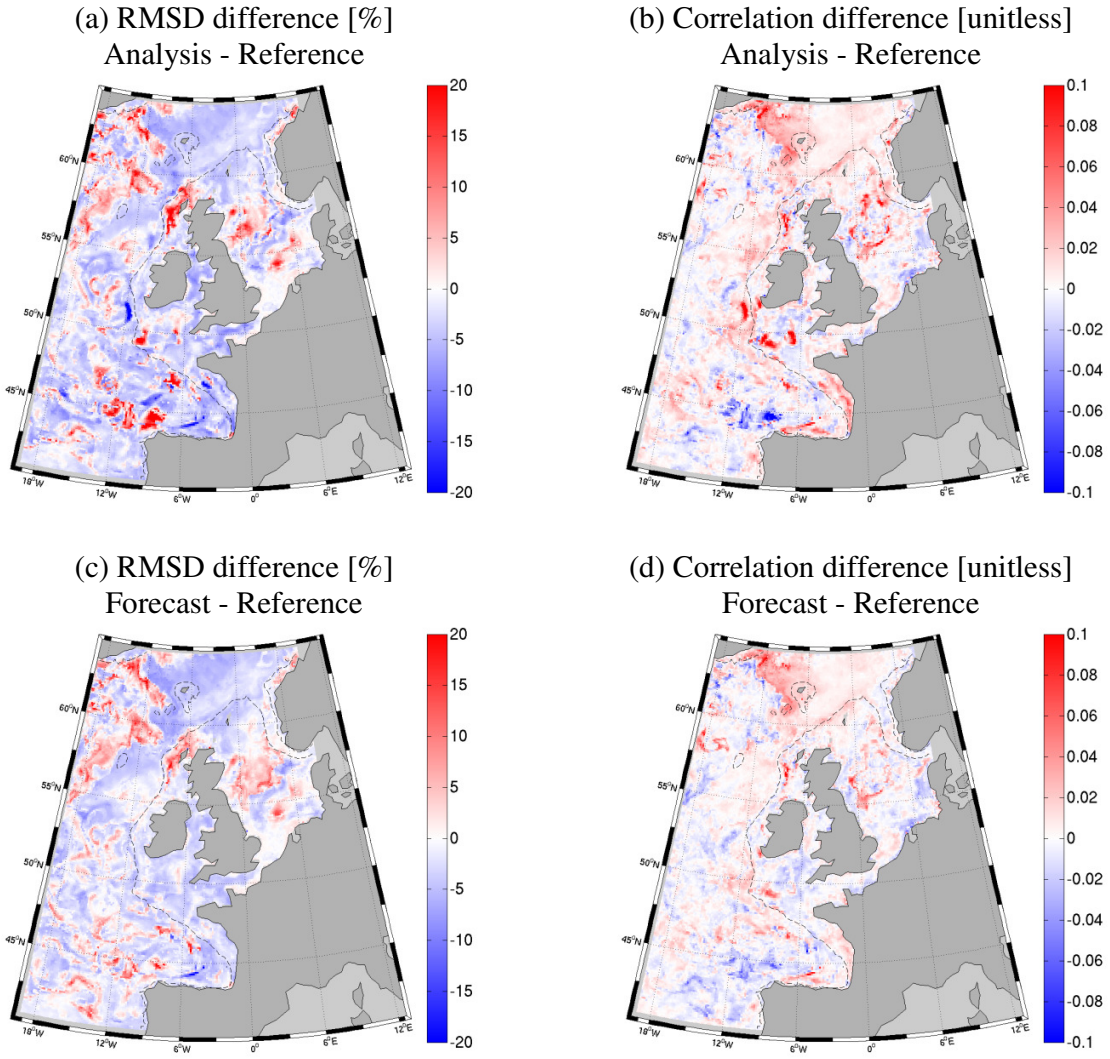

388

389 **Figure 6** Differences between the skill of the assimilation and reference runs in simulating the
390 time series of chlorophyll concentrations at each point of the model domain. The top panels (a)
391 and (b) show the differences computed for the assimilative analysis, the bottom panels (c) and
392 (d) show the differences for the assimilative forecasts. The panels on the left (a) and (c) show the
393 percentage differences of the root mean square deviations (RMSDs), normalized by the RMSD
394 of the reference simulation; the panels on the right (b) and (d) show the difference between the
395 correlations computed from the assimilative and reference outputs. The dashed line represents
396 the 200 m isobath delimiting the shelf region for convention.

Considering the skill over time, both the assimilative forecasts and analysis had lower errors than the reference simulation throughout most of the reanalysis period (Figure 7). Reduction of the RMSD by assimilation were in general more frequent in the spring and summer seasons (see for example summer 2005), while in winter changes were often negligible (for example winter 2005/06). Noticeable reductions of the RMSD were obtained in December 2000, 2001and 2008, but these results were less robust, because in December typically only a small amount of data was available for assimilation and validation, due to cloud cover and to the low solar zenith angle at the latitudes of the study region. In general, re-initialization at the analysis step improved the subsequent forecast. However, in some instances, the forecasts were worse than the reference, and the analysis could only mitigate the deterioration of the simulation (e.g. in spring-summer 1998). Similar temporal patterns of skill improvement and deterioration were found in the time series of reference, analysis and forecast correlations with the ocean color data (not shown).

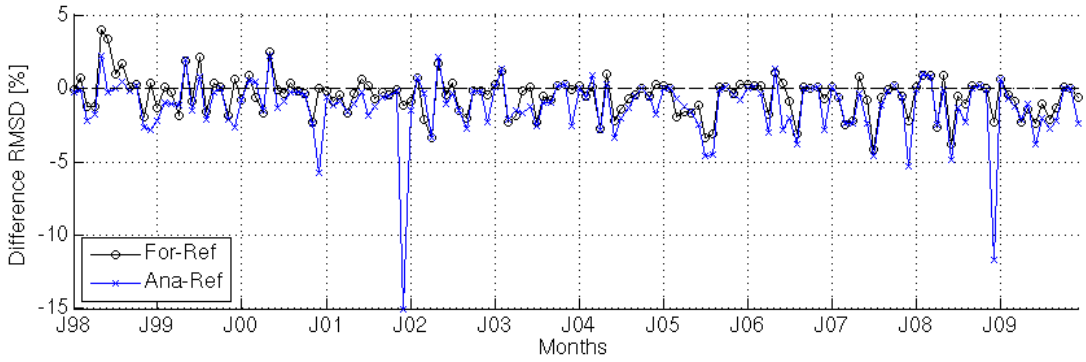

Figure 7 Differences between the RMSD of the assimilative and reference outputs in estimating the spatial distributions of chlorophyll in the entire North East Atlantic, at each month of the period 1998-2009 (J is January). The two lines represent the differences of the assimilative forecasts (For, circles) and analysis (Ana, crosses) with respect to the reference (Ref).

Improved estimates of the assimilated data were expected from the analysis, and essentially this achievement indicates that the data assimilation algorithm was implemented correctly [*Gregg et al.*, 2009]. However, the improved skill from the one-month forecasts shown in Figures 6 and 7 was not obvious, since forecasting the not-yet-assimilated data is a challenging task even for state-of-the-art operational systems [*Ford et al.*, 2012; *Teruzzi et al.*, 2014]. In principle, the re-initialization of the assimilated variable closer to the data should improve also the forecast of the next available data, with respect to the reference run. However, re-initialized biogeochemical fields often tend to be "forgotten" and to converge back to the reference simulation because of the effect of hydrodynamics, forcing, boundaries values, biogeochemical processes [*Allen et al.*, 2003; *Friedrichs et al.*, 2006; *Teruzzi et al.*, 2014]. In addition, multivariate analysis can produce values that are not consistent with the simulated model dynamics, e.g. outlier nutrient values, thus developing simulation instabilities that can lead the forecast to deteriorate both the assimilated and un-assimilated variables [*Gregg et al.*, 2009; *Ciavatta et al.*, 2011]. These potential shortcomings of assimilation may explain the limited areas of skill deterioration pointed out in Figure 6, such as in the complex coastal zones.

3.2 Skill in matching the in situ data

In general, the reanalysis provided skilled estimates of the in situ physical and biogeochemical data in the North East Atlantic in the years 1998-2009. The output captured qualitatively the central position and dispersion of most of the observations, for most of the variables (Figure 8). The reanalysis-to-observation match-ups are well aligned along the bisector line of the plots for temperature, salinity and dissolved oxygen, indicating a skilled

representation of both the magnitude and variability of the observations. The match-ups for phosphate, silicate and nitrate indicate a general overestimation of nutrients, while the reanalysis underestimated (overestimated) low (high) pCO_2 data. Interestingly, in the plots of nutrients, two areas of elevated data density are distinguishable at low and high concentrations, representing the summer and winter conditions respectively, which in turn are related to the seasonal cycle of primary production and stratification. This pattern of nutrients is captured by the reanalysis, though the winter concentrations are overestimated. Match-ups for in situ chlorophyll and ammonia are scattered in the plot, indicating that the high variability of these data was not described by the reanalysis. Finally, the reanalysis was able to represent the magnitude of the pH data, but not their fluctuations.

The quantitative metrics confirm the high skill of the reanalysis in estimating temperature, salinity and dissolved oxygen (e.g., both the Pearson and Spearman correlations were higher than 0.7) (Figure 9). The skill for the majority of other variables was relatively high when robust metrics were used (Fig. 9c), rather than the metrics based on the Gaussian assumption (Figs. 9a and 9b). A clear example is *in situ* chlorophyll, which is much closer to the center in the robust Target diagram 9c, rather than in the standard Target 9b. Chlorophyll, phosphate, nitrate and silicate all reached correlations 0.6 or higher when the Spearman rank correlation was computed (9c). Robust metrics make the comparison of the variability of observations and estimates sounder by using percentiles of the distributions (interquartile and median), which reduce the impact of outliers. For example, outlier data of nutrients imply that the standard deviations are higher for the observations than for the reanalysis, leading these variables to stay below the unit radius in the Taylor diagram in Fig. 9a, and on the left side of the Target diagram in Fig. 9b; however nutrients shifted to the right side of the robust Target diagram in Fig 9c, since the

462 estimates fluctuated more than the data when less weight is given to the outlier observations.
463 Considering the robust skill metrics, the pCO_2 correlation with data is not negligible (~0.4) and
464 the overestimated variability and the bias are within the range of the errors for the other
465 variables. The same holds for pH, though the low Spearman correlation confirms that the model
466 captures the magnitude of this variable, but not its variability.

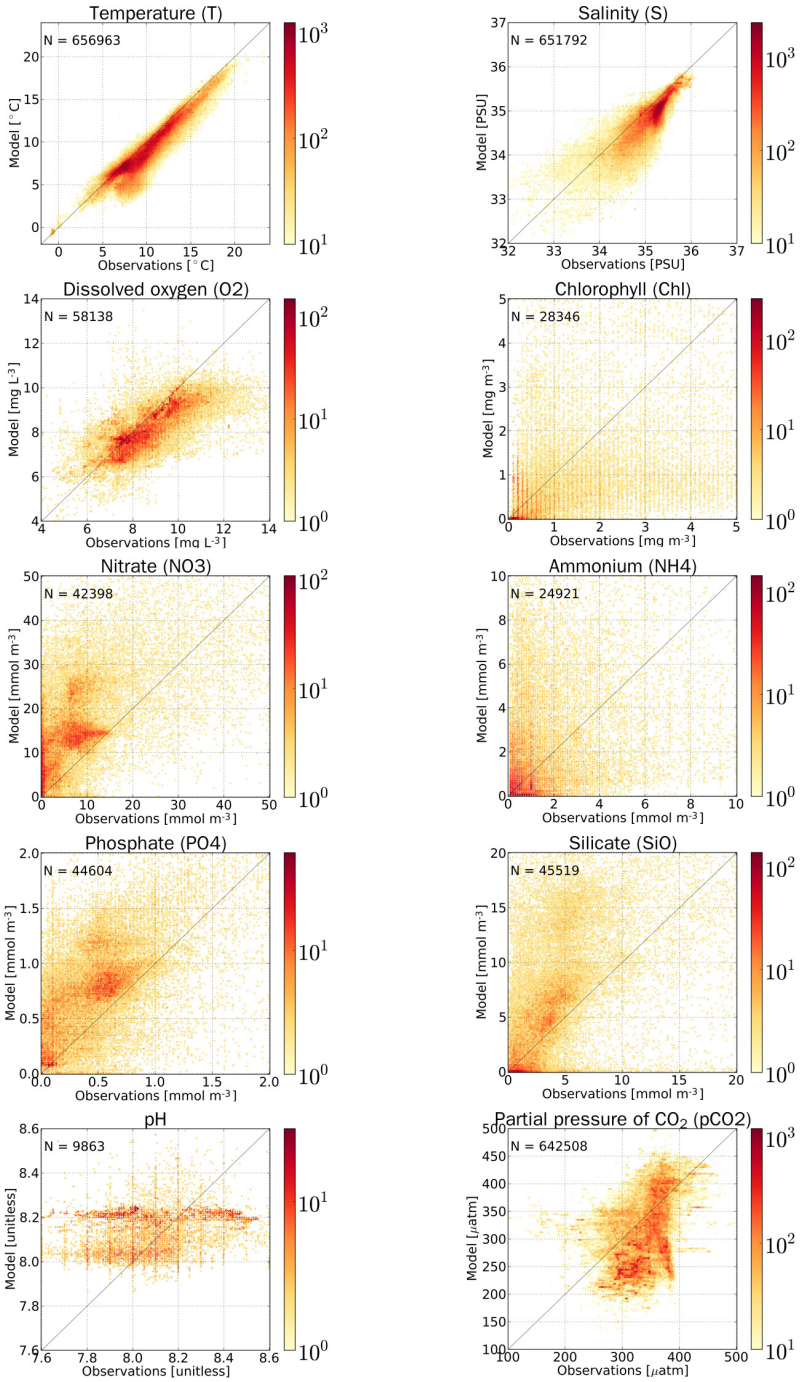

Figure 8 Density plots of the reanalysis output (y-axis) versus in situ observations (x-axis) measured in the North East Atlantic in the years 1998-2009. The colors represent the density (i.e. number of overlapping observations) in logarithmic scale (note the different scales for the variables). N is the total number of match-ups. The notation of the variables in the plot titles is applied also in Figure 9.

The skill of the reanalysis for the unassimilated variables in Figure 9 was not significantly different from the skill of the reference run (not shown). This means, on the one hand, that the model itself performs satisfactorily in estimating in situ data available in the North East Atlantic. On the other hand, it means that improved ocean color estimates did not come at the cost of worsening the estimates of the other model variables. This is not always the case, since ocean color assimilation can cause unrealistic changes in biogeochemical variables which are not assimilated, reducing the model skill and creating feed-back effects that eventually can blow the simulations [*Fontana et al.*, 2013, *Gregg et al.*, 2009; *Ciavatta et al.*, 2011; *Ford et al.*, 2012; *Terruzzi et al.*, 2014]. In our application, two factors can have contributed to the low impact of assimilation on the skill metrics for unassimilated variables, namely the location of the *in situ* sampling points and the frequency of the assimilation of satellite data. Most of the match-ups with *in situ* data occur in coastal case II waters, where ocean color error is higher (Figure 3c) and therefore assimilative corrections are smaller than in the open ocean. This is suggested also by the sensitivity analysis of an analogous assimilation system applied in a subdomain of the study region [*Ciavatta et al.*, 2011]. The relatively low assimilation frequency imposed by the high computational cost of the multivariate ensemble method – i.e. monthly assimilation, compared for example with daily assimilation allowed by the univariate relaxation method in *Rousseaux and Gregg* [2015] – also constrained our reanalysis to impact more strongly on the skill for unassimilated variables.

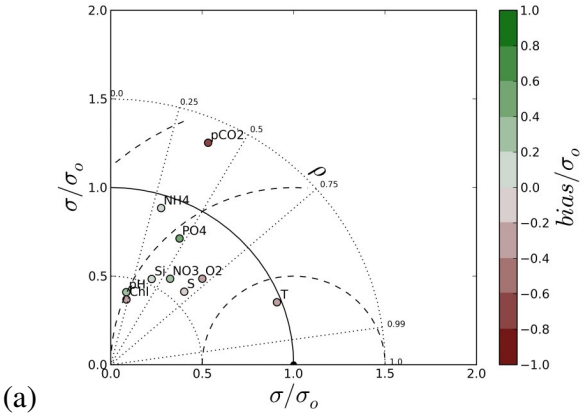

(a)

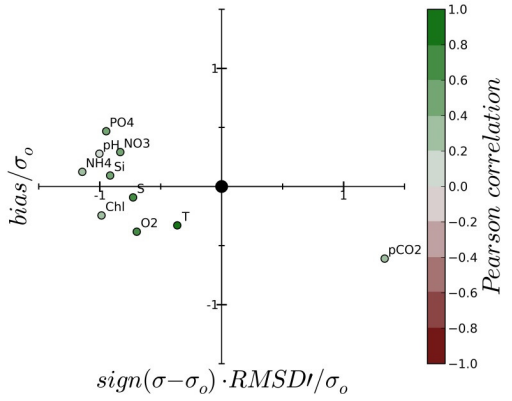

(b)

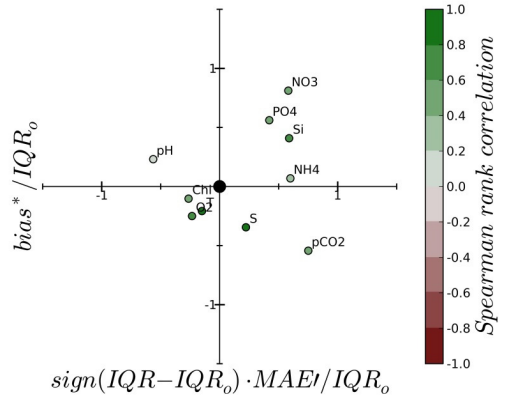

(c)

492 **Figure 9** Skill of the reanalysis in estimating in situ data of ten physical and biogeochemical
493 variables observed in North East Atlantic in the years 1998-2009. Gaussian-base metrics are used
494 in the Taylor (a) and Target (b) diagrams, while robust metrics are shown in the Target diagram
495 (c). The metrics are defined in Section 2.4, the notation of the variables is defined in Fig. 8.

3.3 Case study I: assessment of oxygen deficiency in shelf bottom waters

Dissolved oxygen concentration is an essential climate variable [*Bojinski et al.*, 2014], a threat to aquatic life at low concentrations [*Vaquer-Sunyer and Duarte*, 2008], and an indicator of eutrophication regulated by international legislation [*OSPAR*, 2013]. The first case study demonstrates that the reanalysis can provide an error-characterized assessment of this indicator. It shows that the bottom of the North West European shelf has large areas at risk of oxygen deficiency (Figure 10), namely the south North Sea, Celtic Sea, Armorican shelf, coastal zones in Scotland, West Ireland and English Channel, but we did not identify anoxic situation in any of these cases. In all the above regions, the reanalysis decadal dataset includes at least one daily value of dissolved oxygen below the concentration of 6 mg/L, but still above 2 mg/L; these are the thresholds of oxygen deficiency and anoxia, respectively, defined by the OSPAR Commission for safeguarding the ecosystem of North East Atlantic [*OSPAR*, 2013].

The extension of the vulnerable area is noticeably larger if we apply a conservative criteria of at least 1% confidence on oxygen deficiency (Figure 10b, red plus yellow area, ~ 380,000 km^2), rather than a less strict 100% confidence (red area, ~ 340,000 km^2). A 1% confidence means that just one of the one-hundred ensemble members estimates daily oxygen below the threshold of 6 mg/L in the bottom layer, while 100% confidence means that all one hundred estimate oxygen below 6 mg/L. The more conservative 1% criterion extends the borders of the vulnerable regions (see e.g. in the Celtic Sea), but it includes also areas otherwise neglected by the assessment, i.e. in the Northern North Sea. Overall, the 1% ensemble criterion extends the area of vulnerability by ~ 40,000 km^2, i.e. an area comparable to the surface of Switzerland.

519

(a) Oxygen: Minimum daily values [mg L^{-1}] (b) Areas vulnerable to oxygen deficiency

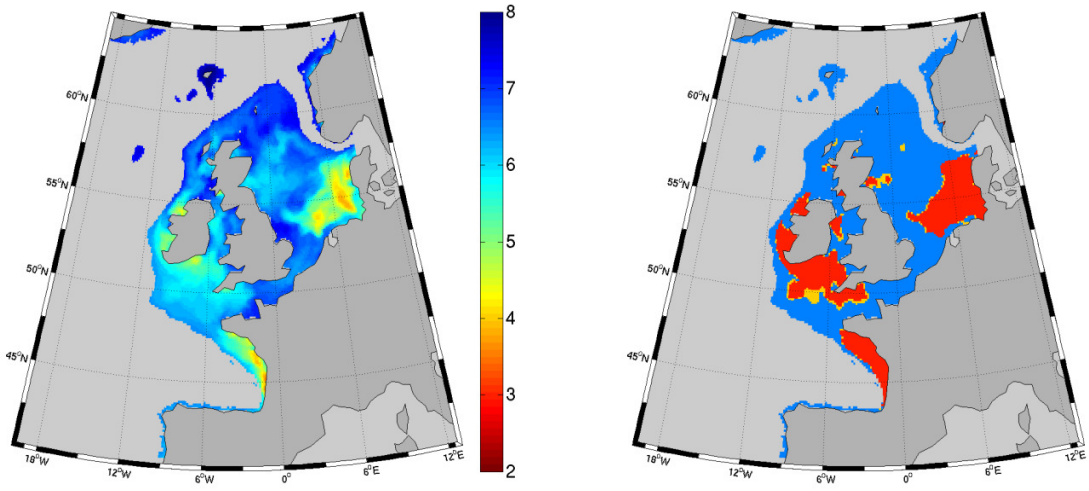

520

521 **Figure 10** (a) Minimum daily values of dissolved oxygen simulated by the ensemble median
522 at the bottom of the shelf in the years 1998-2009 (bathymetry < 200 m) and (b) map of the areas
523 at risk of oxygen deficiency, i.e. with at least one daily value in 1998-2009 below the threshold
524 of 6 mg L^{-1}. In (b), yellow color represent deficient areas at 1% confidence level (i.e. at least one
525 member of the ensemble signals oxygen deficiency), red represents 100% confidence (all the
526 one-hundred members signal deficiency), and blue the areas of the shelf with concentration
527 higher than 6 mg L^{-1} at 100% confidence.

528

529 The simulated absolute minimum values of oxygen at each day, at any point within the risk
530 area, have a clear seasonal pattern and no evident trend in the years 1998-2009 (Figure 11). The
531 lowest values (3.5-4 mg/L) are typically reached in August/September, they increase sharply in
532 autumn and return to not-deficient values in spring. The bottom minima occurred with higher
533 frequency in the Armorican shelf near the Gironde and Loire estuaries, and in the German Bight.
534 The concentrations never descended below the hypoxia threshold; however, they reached

persistent low values that were found lethal for some benthic species, e.g. 4.6 mg/L were found lethal for some fishes and mollusks in the review by *Vaquer-Sunyer and Duarte* [2008]. This low value was reached at both the 1% and 100% confidence levels (Figure 11).

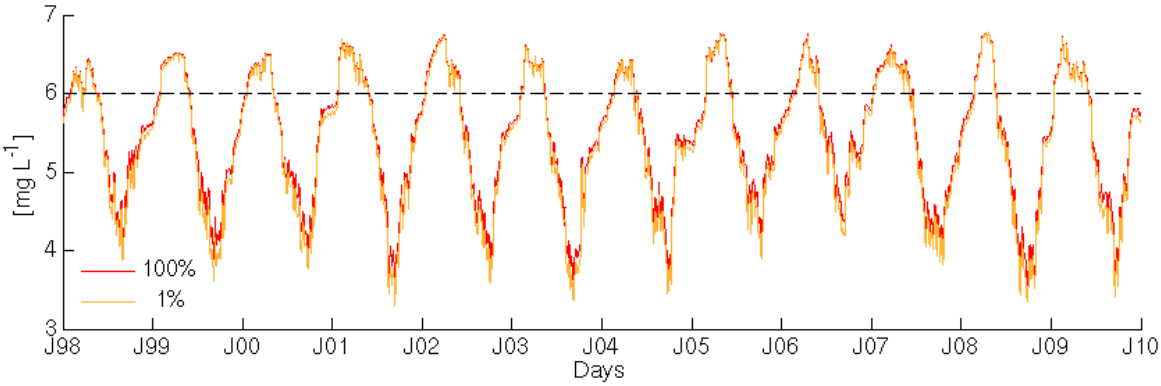

Figure 11 Time series of absolute minimum concentration of dissolved oxygen simulated within the vulnerable area shown in Figure 10; yellow and red lines represent the minimum values at 1% and 100% confidence level, respectively.

The location of vulnerable areas identified in Figure 10 matches the global map of hypoxia and eutrophication areas in *Rabalais et al.* [2014] (http://www.wri.org/our-work/project/eutrophication-and-hypoxia/interactive-map-eutrophication-hypoxia) and compares reasonably well with regional studies for the Celtic Sea [*O'Boyle and Nolan*, 2010], North Sea [*Greenwood et al.*, 2010] and Armorican shelf [*Charria et al.*, 2014]. The latter work presents a continuous, two-year long time series of oxygen data that matches well the seasonal pattern shown in Figure 11. The authors showed that oxygen solubility, seasonal stratification of the water column and bacterial remineralization of organic matter are the potential triggers of low bottom oxygen concentrations in the region, particularly in summer [e.g. *O'Boyle and Nolan*,

553 2010, *Greenwood et al.*, 2010]. Our simulation extend these findings to the scale of the whole
554 shelf, since we found highly significant anti-correlations between the oxygen series in Figure 11
555 and the daily series of water temperature, bacteria biomass and particulate organic carbon
556 simulated at the same bottom locations (Spearman rank correlations ρ_s = -0.75, -0.59 and -0.63,
557 respectively, $p<0.01$). Furthermore, Figure 11 suggests that oxygen deficiency may occur also in
558 winter months at some shelf locations (e.g. near estuaries). This could not be directly confirmed
559 by measurements collected in the ICES oxygen data base, where the coverage for bottom water
560 in winter is far too low to permit the identification of this phenomenon (www.ices.dk).
561 Therefore, these findings stimulates increasing the extension, frequency and seasonal coverage
562 of European bottom water monitoring for better understanding and predicting oxygen dynamics.
563
564 The soundness of the confidence levels shown in Figures 10 and 11 depends on the proved
565 reliability of the model description of oxygen (Section 3.3), but also on our arbitrary choices in
566 the set-up of the ensemble simulation, for example in the initial ensemble conditions for oxygen
567 (Section 2.2.1). However, dissolved oxygen was neither analyzed nor perturbed systematically in
568 the reanalysis, nor were temperature and salinity, which are the physical drivers of the oxygen
569 solubility in the water column. Thus, the oxygen spread in the ensemble was propagated by
570 biological processes only, which were perturbed through the analysis and perturbation of the
571 other model state variables, as well as through the perturbation of the surface irradiance (Section
572 2.2.1). On the one hand, such propagation of the spread implies that the assimilation system for
573 surface chlorophyll was capable of conveying the assimilated information and the model
574 uncertainty across the simulated trophic structure, and down to the bottom of the water column to
575 affect the simulation of oxygen at depth. On the other hand, it implies also that the range of the

576 confidence level (i.e. the spread of oxygen) would be underestimated if the errors we assumed
577 for the other model variables and irradiance forcing (i.e. the standard deviations of their
578 perturbations) were underestimated in the first instance.

579 Besides dissolved oxygen, the reanalysis output also contains data characterizing the spatial-
580 temporal variability and confidence levels of the other ten variables linked to biogeochemical
581 indicators listed in European legislation [*OSPAR*, 2013], including chlorophyll, nutrients and pH,
582 which are skill-assessed in sections 3.1 and 3.2 (see Appendix 2 for a complete list of the
583 reanalysis output).

584 ### 3.4 Case study II: assessment of atmospheric CO_2 uptake by the shelf

585

586 The reanalysis dataset can be applied to estimate the interannual variability of the shelf uptake
587 of atmospheric CO_2, and to evaluate the confidence levels for such estimates, as shown in this
588 case study. The North East Atlantic is a net sink of atmospheric CO_2 at a high confidence level
589 (Figure 12). The ocean uptake increases from south to the northern colder waters (from ~5 to 15
590 mol C m^{-2} yr^{-1}) and from the coast towards the open ocean. On the shelf, the uptake is typically
591 lower than 5 mol C m^{-2} yr^{-1} (region delimited by the 200 m isobath in Figure 12). Weak sources
592 of CO_2 to the atmosphere (<1 mol C m^{-2} yr^{-1}) were found in the English Channel, Irish sea, and
593 near estuaries. The interannual variability of the fluxes was more homogeneous and smaller than
594 the interannual means, in general (Figure 12b). However, variability and means were comparable
595 in the Irish Sea and English Channel, indicating that these areas can switch from being weak
596 sinks [*Kitidis et al.*, 2012] to weak sources of CO_2 in some years, as a consequence of
597 interannual fluctuations of the ecosystem dynamics (e.g., primary production) and forcing (e.g.,
598 water temperature) [*Marrec et al.*, 2015; *Borges and Frenkignoulle*, 2003]. The uncertainty in

599 the fluxes was in general lower than their average values, indicating that the reanalysis is suitable
600 for assessing flux directions, i.e. defining sink or source zones, at a 90% confidence level.
601 However, in some zones uncertainty and fluxes were comparable low, for example in the English
602 Channel, south North Sea, and Norwegian coast (Figure 12d). These areas should be considered
603 flux-neutral at 90% confidence, like the English Channel that was already classified a "not-
604 significant-sink" by *Borges and Frankignoulle* [2003].
605

606

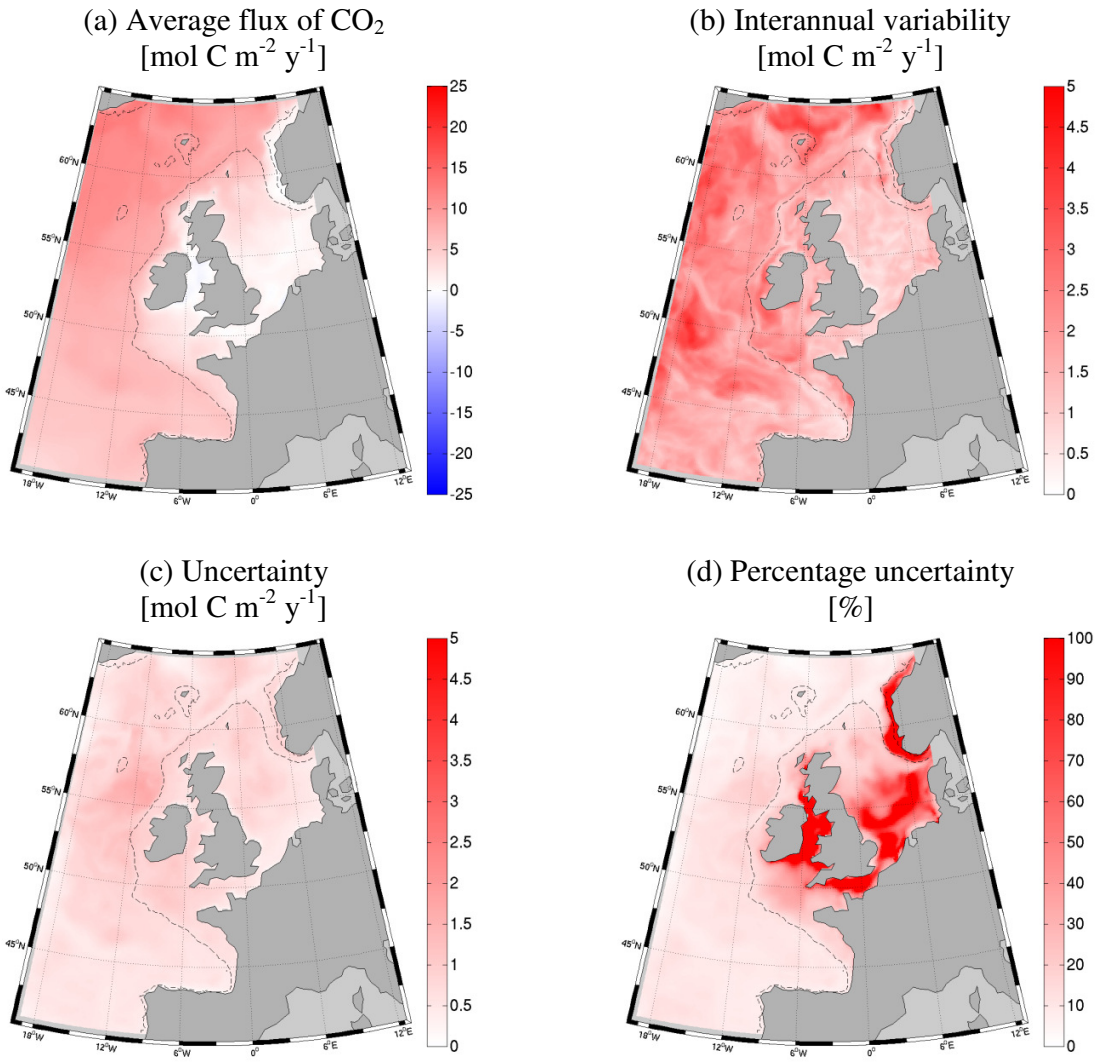

607 **Figure 12** Air-sea flux of CO_2: (a) average yearly values in 1998-2009 (positive values
608 represent sink, negative values source); (b) interannual variability as range maximum-minimum
609 of the yearly values; (c) uncertainty as average value of the range between the 95th-5th percentiles
610 of the ensemble. Map (d) shows the uncertainty in (c) normalized by the average in (a). The
611 dashed line represents the 200 m isobath delimiting the shelf region for convention.

612

613

614 The overall annual uptake of carbon dioxide in the shelf region was 41 Tg C y^{-1} on average in
615 the period 1998-2009, but this value has an uncertainty of ±5 Tg C y^{-1} (i.e. ~25% of the average),
616 at 90% confidence level, and with an interannual variability of ~20% (Figure 13, Table 1). These
617 estimates are coherent with previous literature findings (Table 1). An estimate of the average
618 obtained with a comparable model, but referred to the years 1989-2004, lie within the range
619 found in this study [*Wakelin et al.*, 2012]. Our average value was higher than the ones provided
620 for the North Sea only [*Thomas et al.*, 2005] and for the European shelf-seas altogether [*Borges*
621 *et al.*, 2006], but they overlap with the uncertainty range in the Gulf of Biscay [*Chen and Borges*,
622 2009].

623 The interannual variability of the yearly uptake of CO_2 ranged between 36-42 Tg C y^{-1} (Table
624 1 and Figure 13), and we found it was related to the interannual variability of the gross primary
625 production (Spearman rank correlation ρ_s = 0.72, $p<0.01$), rather than to the interannual
626 fluctuations of sea surface temperature (not-significant rank correlation). These results agree
627 with *Wakelin et al.* [2012], who suggested that biological processes exert a stronger effect than
628 temperature on the air-sea flux of CO_2 in the study region.

629 Our estimate of the uncertainty of the total flux (±5 Tg C y^{-1}, i.e. 25% of the average) appears
630 sound, considering that it is coherent with the error assessed for pCO_2 observations (percentage
631 RMSD=~20%, Section 3.2), and it is comparable in percentage to the range of uncertainty
632 estimated by Thomas et al., 2005 (~22%, Table 1). The estimated uncertainty of the flux is
633 arguably linked to the uncertainty of primary production (see above rank correlation), which is
634 however constrained rather directly by the corrections of ocean color assimilation. In addition,
635 the estimated uncertainty of the flux was larger than the arbitrary perturbations imposed on

636 dissolved organic carbon (DIC) in the assimilative initialization (1%, Section 2.2.1), suggesting
637 that the subjective initial perturbation of DIC did not strongly constrain the estimated uncertainty
638 of its flux at the atmosphere interface. Our estimate of the uncertainty of the CO_2 flux is limited
639 by not accounting for the error in the un-perturbed temperature and salinity, which however are
640 simulated skillfully by the model system (Section 3.2).

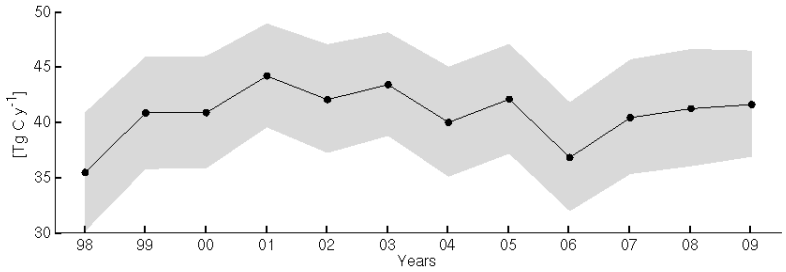

641

642 **Figure 13** Interannual variability and confidence of the yearly sink of atmospheric CO_2 in the
643 North West European shelf (bathymetry shallower than 200 m); the grey band represents the
644 range between the 95th and 5th percentiles of the reanalysis ensemble.

645

Table 1 Air-sea fluxes of CO_2 in the North West European shelf (positive values indicate sinking), ranges of their interannual variability and uncertainty. The total fluxes were computed for the shelf region with bathymetry shallower than 200 m represented in Figure 12 (1.2 million km^2). Previous reference values are reported for comparison.

	mol C m^{-2} y^{-1}	Tg C y^{-1}	References
Average	2.8	41	This work
		39.6	Same domain as this work [*Wakelin et al.*, 2012]
	1.38		North Sea only [*Thomas et al.*, 2005]
	1.9		European shelf seas altogether[*Borges et al.*, 2006]
Interannual range	2.1-3.5	36-42	This work
		37.2-42	Standard deviation 2.4 Tg C y^{-1} [*Wakelin et al.*, 2012]
Uncertainty range	2.4-3.1	36-46	This work
	1.7-2.91		Gulf of Biscay [*Chen and Borges*, 2009]
	1.2-1.5		North Sea only [*Thomas et al.*, 2005]

646

647 The provision of sound estimates of the uncertainty of carbon fluxes based on assimilative
648 ensemble simulations is an added value of the reanalysis with respect to the reference simulation.
649 The relatively large range of uncertainty estimated here calls for the development and
650 assimilation of ocean color products with higher accuracy for type-2 shelf-sea waters, so that the
651 reanalysed air-sea fluxes of carbon dioxide can be constrained more strongly. The assimilation of
652 optical data from ocean color could help, because such data have a lower error than chlorophyll
653 in shelf seas, and they can constrain directly a larger number of variables that are optically active
654 and contribute to carbon fluxes, such as particulate and colored dissolved organic matter
655 [*Ciavatta et al.*, 2014]. A further promising option is including pCO_2 assimilation in shelf-sea
656 reanalysis, since this arguably improved the estimation of the air-sea flux of CO_2 in an annual
657 simulation of the global ocean biogeochemistry in the work by *While et al.* [2012].
658 The reanalysis dataset contains values and confidence ranges of a large number of
659 biogeochemical fluxes which are useful to investigate nutrient cycles and ecosystem processes in
660 the North West European shelf-sea (see the list in Appendix 2).
661

662 **4 Conclusions**
663

664 The reanalysis of the North East Atlantic biogeochemistry provided a unique decadal dataset
665 that has considerable skill in approximating ocean observations, and that can enhance the
666 understanding and management of the North West European shelf ecosystem, in relation to
667 eutrophication and fluctuations of the carbon cycle.

668 Importantly, the reanalysis comes with confidence levels that quantify the uncertainty of the
669 biogeochemical estimates. The crucial implications of this supplementary information were
670 evident in two case studies, where we assessed that:

671 • An area as large as 340,000 km^2 was vulnerable to oxygen deficiency at the bottom of the
672 North West European shelf, but additional 40,000 km^2 are included when using a strict 1%
673 confidence criteria;

674 • The North West European shelf is a net sink of atmospheric CO_2, but our simulated
675 uptake can range between 36-46 Tg C yr^{-1}, when applying a 90% confidence level for the
676 estimates.

677 The confidence levels provided here are an added value of the reanalysis with respect to the
678 model output alone, because estimates of reliability are much needed for model applications in
679 marine policy [*Hyder et al.*, 2015]. For example, provision of percentile confidence level is
680 required for eutrophication indicators inferred from monitoring programs [*OSPAR*, 2013], but
681 quantification of uncertainty is a crucial gap when such indicators are estimated through model
682 simulations [*Piroddi et al.*, 2015]. The ensemble-based reanalysis presented here can help with
683 tackling this gap in our knowledge of the North West European shelf, and the same
684 methodological approach can be applied with other shelf-sea models running on adequate high
685 performance computing facilities. Further insights into the confidence in simulated ecosystem
686 indicators and biogeochemical fluxes – including the contribution of uncertainty in
687 hydrodynamics not accounted for here – can be achieved using an ensemble of different
688 biogeochemical models [*Lenhart et al.*, 2010; *Skogen et al.*, 2014; *Anav et al.*, 2013]. The use of
689 our reanalysis in such a type of ensemble is the subject of our ongoing work within the Marine
690 Environment Monitoring Service of the European Copernicus programme.

691 Finally, to our knowledge this is the first reanalysis that is taking advantage of the by-pixel
692 estimates of the errors of the assimilated ocean color product, decreasing the level of subjectivity
693 often applied in biogeochemical data assimilation [*Ciavatta et al.*, 2014]. However, the product
694 we used was derived primarily for case-I waters. We expect that further advantages for
695 biogeochemical reanalysis in shelf-seas will derive from the availability of long-term, integrated
696 products for case-I and II waters, e.g. from the current efforts of the Ocean Colour Climate
697 Change Initiative of the European Space Agency.
698 The reanalysis product presented in this paper is available for download and applications at
699 the data portal http://portal.marineopec.eu/
700

701 **Acknowledgments and Data**

702

703 This work was supported by the UK NERC through the National Centre for Earth
704 Observation (NCEO) and the Atlantic BiogeoChemical (ABC) Fluxes Project of the RAPID-
705 AMOC Programme, by the EC FP7 Operational Ecology (OPEC), by the EU-FP7 MyOcean
706 project, and by the Project NOWMAPS of the European Copernicus Marine Environment
707 Monitoring Service. This work contributes to the European Space Agency's Climate Change
708 Initiative – Ocean Colour (http://www.esa-oceancolor-cci.org). The work used the UK National
709 Supercomputing Service "ARCHER". The in situ data for validation were downloaded from the
710 ICES database (http://ices.dk/marine-data) and SOCAT database (http://www.socat.info/). The
711 authors thank Dr. Shubha Sathyendranath for discussion on the use of the ESA's CCI Ocean
712 Colour product, and Dr. Yuri Artioli for discussion on the use of the North East Atlantic
713 ecosystem model.

Appendix 1. Set-up of the assimilated observations and errors

Daily OC_CCI data of chlorophyll concentration at 4 km resolution were un-biased, scaled onto the model grid (1/6° in longitude, and 1/9° in latitude, Section 2.1) and merged in five day composites following the procedure described in this section. Bias and RMSD of the OC_CCI data are provided in base-10 logarithm, while chlorophyll data are provided as concentrations in mg m^{-3} [*Grant et al.*, 2015]. Therefore, in the reanalysis, central and dispersion parameters of the data distributions were back-and-forward transformed from concentration units to natural logarithm, which is used in the analysis step of assimilation (Section 2.2).

Given the chlorophyll concentration at pixel *p*, and day *t* ($y_{p,t}$), and base-10 logarithmic values of the bias ($\delta_{10,p,t}$) and mean-square-deviation $\Delta^2_{10,p,t}$ we approximated per-pixel values of the base-10 logarithm of the standard deviation of the data as [*Grant et al.*, 2015]:

$$\sigma_{10,p,t} = \sqrt{\left|\Delta^2_{10,p,t} - \delta^2_{10,p,t}\right|} \qquad \text{A1.1}$$

Assuming that $y_{p,t}$ represents the mean value of the log-normal distribution of chlorophyll [e.g., *Campbell*, 1995], the mean value of the log-transformed distribution ($\mu_{10,p,t}$) was calculated (eq. 39 in *Mood et al.* [1974] and *Campbell* [1995]):

$$\mu_{10,p,t} = log_{10}(y_{p,t}) - 1/2 \cdot \sigma^2_{10,p,t} \cdot log_e(10) \qquad \text{A1.2}$$

And the bias-corrected value $\mu'_{10,p,t}$ was computed:

$$\mu'_{10,p,t} = \mu_{10,p,t} + \delta_{10,p,t} \qquad \text{A1.3}$$

taking account of the OC_CCI convention of negative values of bias ($\delta_{10,p,t} < 0$) for ocean color overestimating actual concentrations [*Grant et al.*, 2015].

735 The un-biased, scaled, five-day composite at each model grid cell c, $\mu'_{10,c}$,was computed by
736 averaging in space and time the bias-corrected data:

737 $$\mu'_{10,c} = \frac{1}{T \cdot N} \cdot \sum_{t=1}^{T} \sum_{p=1}^{N} \mu'_{10,p,t} \quad \text{A1.4}$$

738 Where T=5 is the number of days, while the number of pixels included in a cell of the model
739 grid is N, which varies in space and time depending on the coordinates of the cell and the
740 number of missing observations.

741 Similarly, the RMSD and bias of the cell composite were computed [*Grant et al.*, 2015]:

742 $$\Delta^2_{10,c} = \frac{1}{T \cdot N} \cdot \sum_{t=1}^{T} \sum_{p=1}^{N} \Delta^2_{10,p,t} \quad \text{A1.5}$$

743 $$\delta_{10,c} = \frac{1}{T \cdot N} \cdot \sum_{t=1}^{T} \sum_{p=1}^{N} \delta_{10,p,t} \quad \text{A1.6}$$

744 And the standard deviation of the cell composite was approximated [*Grant et al.*, 2015]:

745 $$\sigma_{10,c} = \sqrt{\left| \Delta^2_{10,c} - \delta^2_{10,c} \right|} \quad \text{A1.7}$$

746 We changed the base of the mean and variance of the distributions to natural logarithm by
747 using mathematical properties [*Campbell*, 1995]:

748 $$\mu'_{e,c} = \mu'_{10,c} \cdot log_e(10) \quad \text{A1.8}$$

749 $$\sigma^2_{e,c} = \sigma^2_{10,c} \cdot [log_e(10)]^2 \quad \text{A1.9}$$

750 These parameters were used in the analysis step of assimilation to compute pseudo-random
751 Gaussian distributions of the observations (Section 2.2). In addition, the mean value (y'_c) and
752 standard deviation (s_c) of the unbiased log-normal distribution of chlorophyll, in concentration
753 units, were obtained from the logarithmic mean and variance in eq. A1.8 and A1.9, by using
754 mathematical properties of log-normal distributions (see eq. 39 in *Mood et al.* [1974]):

755 $$y'_c = e^{(\mu'_{e,c} + \frac{\sigma^2_{e,c}}{2})} \quad \text{A1.10}$$

$$s_c = \sqrt{(e^{\sigma^2_{e,c}} - 1) \cdot e^{(2\mu'_{e,c} + \sigma^2_{e,c})}} \qquad \text{A1.11}$$

These are the parameters used in the presentation of the assimilated data in Figure 3.

Appendix 2. The reanalysis dataset

The reanalysis dataset is available in digital files produced in Network Common Data Form (NetCDF) version 4 (http://www.unidata.ucar.edu), following the standard convention "Climate and Forecast" metadata CF-1.5 (http://cfconventions.org/). Separated files contain different statistics of the reanalysis ensemble (median, mean, 5th percentile, 95th percentile, minimum, maximum), for daily and monthly means of pelagic and benthic variables and fluxes listed in Tables A2.1-A.2.4. An extensive description of such variables and fluxes was provided by *Butenschön et al.* [2015]. The full reanalysis dataset has a size of ~12 Tera bytes. A subset of the regridded dataset can be visualized, processed and downloaded at the data portal http://portal.marineopec.eu/, while the full dataset is available on request to the corresponding author.

771

Table A2.1. List of pelagic variables available as daily means in the reanalysis output files. The last column points out variables linked to ecosystem indicators specified by the OSPAR Convention [*OSPAR*, 2013].

Notation	Unit	Description	Ind
netPP	tons C/d^{-1}	Net primary production	
pCO2w	µatm	Partial pressure of CO_2 in water	
pH	1	pH	X
P1c	mg C m^{-3}	Diatoms carbon	
P2c	mg C m^{-3}	Nanophytoplankon carbon	
P3c	mg C m^{-3}	Picophytoplankton carbon	
P4c	mg C m^{-3}	Microphytoplankton carbon	
Chl1	mg C m^{-3}	Diatoms chlorophyll	X
Chl2	mg C m^{-3}	Nanophytoplankon chlorophyll	X
Chl3	mg C m^{-3}	Picophytoplankton chlorophyll	X
Chl4	mg C m^{-3}	Microphytoplankton chlorophyll	X
N3n	mmol m^{-3}	Nitrate	X
N4n	mmol m^{-3}	Ammonium	X
N1p	mmol m^{-3}	Phosphate	X
N5s	mmol m^{-3}	Silicate	X
O2o	mmol m^{-3}	Oxygen	X
EIR	W m^{-2}	Irradiance	
B1c	mg C m^{-3}	Bacteria carbon	
Z4c	mg C m^{-3}	Mesozooplankton carbon	
Z5c	mg C m^{-3}	Microzooplankton carbon	
Z6c	mg C m^{-3}	Heterotrophic Nanoflagellates carbon	
R1c+R2c+R3c	mg C m^{-3}	Total DOC	
R4c+R6C+R8c	mg C m^{-3}	Total POC	
L2c	mg C m^{-3}	Calcite	
ETW	°C	Temperature	X
x1X	psu	Salinity	
rholocal	kg m^{-3}	Sea water density	
nuv	m^{-2}/s	Vertical turbulent diffusivity	
oChl	mg Chl	Total chlorophyll averaged over the optical depth	
opticalDepth	m	Optical Depth	
fairmg	mg C m^{-2}	Air – sea flux of CO_2	

772

Table A2.2. List of pelagic variables available as monthly means in the reanalysis output files.

Notation	Unit	Description
grossPP	tons C/d^{-1}	Photosynthesis (gross production)
PResp	tons C/d^{-1}	Phytoplankton respiration
ZResp	tons C/d^{-1}	Zooplankton respiration
BResp	tons C/d^{-1}	Bacterial respiration
TotA	umol/kg	Total alkalinity
bioalk	umol/kg	Bioalkalinity
O3c	mmol m^{-3}	Dissolved organic carbon (DIC)
R1c	mg C m^{-3}	Labile dissolved organic carbon (DOC)
R2c+R3c	mg C m^{-3}	Recalcitrant DOC
R4c	mg C m^{-3}	Small size particulate organic carbon (POC)
R6c	mg C m^{-3}	Medium Size POC
R8c	mg C m^{-3}	Large size POC
P1n	mmol N m^{-3}	Diatoms chlorophyll
P2n	mmol N m^{-3}	Nanophytoplankon nitrogen
P3n	mmol N m^{-3}	Picophytoplankton nitrogen
P4n	mmol N m^{-3}	Microphytoplankton nitrogen
P1p	mmol P m^{-3}	Diatoms nitrogen
P2p	mmol P m^{-3}	Nanophytoplankon phosphate
P3p	mmol P m^{-3}	Picophytoplankton phosphate
P4p	mmol P m^{-3}	Microphytoplankton phosphate
P1s	mmol Si m^{-3}	Diatoms silicate
BGE	1	Bacterial growth efficiency
B1n	mmol N m^{-3}	Bacteria nitrogen
B1p	mmol P m^{-3}	Bacteria phosphate
netB1	tons C d^{-1}	Bacterial production
fPXZXc	tons C d^{-1}	Zooplankton Predation on Phytoplankton
fBXZXc	tons C d^{-1}	Zooplankton Predation on Bacteria
fRXZXc	tons C d^{-1}	Zooplankton Predation on Particulate Matter
fPXRPc	tons C d^{-1}	Phytoplankton Excretion and Mortality to POC
fZXRPc	tons C d^{-1}	Zooplankton Excretion and Mortality to POC
fPXRDc	tons C d^{-1}	Phytoplankton Excretion to DOC
fZXRDc	tons C d^{-1}	Zooplankton Excretion to DOC
fBXRDc	tons C d^{-1}	Bacteria Mortality DOC
fRPBXc	tons C d^{-1}	POC uptake by bacteria
fN1PXp	Mmol P d^{-1}	Phosphate Uptake by Phytoplankton
fN3PXn	Mmol N d^{-1}	Nitrate Uptake by Phytoplankton
fN4PXn	Mmol N d^{-1}	Ammonium Uptake by Phytoplankton
fN5PXs	Mmol Si d^{-1}	Silicate Uptake by Phytoplankton
fB1N1p	Mmol P d^{-1}	Phosphate Production by Bacteria
fB1NIn	Mmol N d^{-1}	Ammonium Production by Bacteria
CProd	tons C d^{-1}	Net ecosystem production (Photosynthesis- pelagic respiration)
fRDBXc	tons C d^{-1}	Bacteria uptake of DOC
calc	mgC m^{-3} d^{-1}	Net calcification

773

Table A2.3. List of benthic variables available as daily means in the reanalysis output files.

Notation	Unit	Description
bL2c	mg m^{-2}	Calcite
Y2c	mg m^{-2}	Deposit Feeders, Macrobenthos carbon
Y3c	mg m^{-2}	Suspension / Filter Feeders, Macrobenthos carbon
Y4c	mg m^{-2}	Meiobenthos carbon
H1c	mg m^{-2}	Aerobic Bacteria carbon
H2c	mg m^{-2}	Anaerobic Bacteria carbon
Q1c	mg m^{-2}	Dissolved Detrital carbon
Q6c	mg m^{-2}	Slowly Degradable carbon
Q7c	mg m^{-2}	Available Refractory carbon
K1p	mmol m^{-2}	Benthic Phosphate
K3n	mmol m^{-2}	Benthic Nitrate
K4n	mmol m^{-2}	Benthic Ammonium
K5s	mmol m^{-2}	Benthic Silicate
G2o	mmol m^{-2}	Benthic Oxygen
G3c	mmol m^{-2}	Benthic Carbon Dioxide
G4n	mmol m^{-2}	Benthic Nitrogen Dioxide
Q17c	mg m^{-2}	Buried Refractory Carbon

774

775

776

777

778

779

780

781

Table A2.4. List of benthic variables available as monthly means in the reanalysis output files.

Notation	Unit	Description
wsiO3c	mg C m^{-2} d^{-1}	Diffusion of inorganic carbon from benthic layer
fPelBenC	mg C m^{-2} d^{-1}	Settling and benthic feeding
wsibl2c	mgC m	Calcite precipitation in benthic layer
wsobl2c	mgC m	Calcite dissolution in benthic layer

782

References

Allen, J. I., and P. J. Somerfield (2009), A multivariate approach to model skill assessment, *J. Mar. Sys.*, 76(1), 83-94.Allen, J. I., M. Eknes, and G. Evensen (2003), An Ensemble Kalman Filter with a complex marine ecosystem model: hindcasting phytoplankton in the Cretan Sea, *Ann. Geophys.*, 21(1), 399-411.

Anav, A., P. Friedlingstein, M. Kidston, L. Bopp, P. Ciais, P. Cox, C. Jones, Martin Jung, R. Myneni, and Z. Zhu (2013), Evaluating the land and ocean components of the global carbon cycle in the CMIP5 Earth System Models, *J. Clim.*, 26(18), 6801-6843.

Artioli, Y., J. C. Blackford, M. Butenschön, J. T. Holt, S. L. Wakelin, H. Thomas, A. V. Borges, and J. I. Allen (2012), The carbonate system in the North Sea: Sensitivity and model validation, *J. Mar. Sys.*, 102, 1-13.

Artioli, Y, J. C. Blackford, G. N., R. G. J. Bellerby, S. L. Wakelin, J. T. Holt, M. Butenschön, and J. I. Allen (2014), Heterogeneity of impacts of high CO_2 on the North Western European Shelf, *Biogeosciences* 11(3), 601-612.

Baretta, J. W., W. Ebenhöh, and P. Ruardij (1995), The European regional seas ecosystem model, a complex marine ecosystem model, *Neth. J. Sea Res.*, 33(3), 233-246.

Baretta-Bekker, J. G., J. W. Baretta, and W. Ebenhöh (1997), Microbial dynamics in the marine ecosystem model ERSEM II with decoupled carbon assimilation and nutrient uptake, *J. Sea Res.*, 38, 195-211, doi:10.1016/S1385-1101(97)00052-X.

Bengtsson, L., and J. Shukla (1988), Integration of space and in situ observations to study global climate change, *Bull. Am. Meteorol. Soc.*, 69(10), 1130-1143.

Blackford, J. C. (1997), An analysis of benthic biological dynamics in a North Sea ecosystem model, *J. Sea Res.*, 38(3-4), 213-230.

Bojinski, S., M. Verstraete, T. C. Peterson, C. Richter, A. Simmons, and M. Zemp (2014), The concept of Essential Climate Variables in support of climate research, applications, and policy, *Bull. Am. Meteorol. Soc.*, 95(9), 1431-1443.

Borges, A. V. (2011), Present day carbon dioxide fluxes in the coastal ocean and possible feedbacks under global change, in *Oceans and the atmospheric carbon content*, edited by P. Duarte, J. M. Santana-Casiano, pp. 47-77, Springer, Netherlands.

Borges, A. V., and M. Frankignoulle (2003), Distribution of surface carbon dioxide and air-sea exchange in the English Channel and adjacent areas, *J. Geophys. Res.*, 108(C5).

Borges, A. V., L. S. Schiettecatte, G. Abril, B. Delille, and F. Gazeau (2006), Carbon dioxide in European coastal waters, *Estuarine Coastal Shelf Sci.*, 70(3), 375-387.

Brewin, R. J. W., S. Sathyendranath, D. Müller, C. Brockmann, P.-Y. Deschamps, E. Devred, R. Doerffer, N. Fomferra, B. Franz, M. Grant, S. Groom, A. Horseman, C. Hu, H. Krasemann, Z. Lee, S. Maritorena, F. Mélin, M. Peters, T. Platt, R. Regner, T. Smyth, F. Steinmetz, J. Swinton, J. Werdell, and G. N. White (2015), The Ocean Colour Climate Change Initiative: III. A round-robin comparison on in-water bio-optical algorithms. Remote Sensing of Environment, 162, 271-294. doi:10.1016/j.rse.2013.09.016.

Burchard, H., K. Holding, and M. R. Villareal (1999), GOTM, a general ocean turbulence model. Theory, applications and test cases, Tech. Rep. EUR 18745 EN, European Commission.

Butenschön, M., J. Clark, J. N. Aldridge, J. I. Allen, Y. Artioli, J. Blackford, J. Bruggeman, P. Cazenave, S. Ciavatta, S. Kay, G. Lessin, S. van Leeuwen, J. van der Molen, L. de Mora, L. Polimene, S. Sailley, N. Stephens, and R. Torres (2015), ERSEM 15.06: a generic model for marine biogeochemistry and the ecosystem dynamics of the lower trophic levels, *Geosci. Model Dev. Discuss.*, 8, 7063-7187, doi:10.5194/gmdd-8-7063-2015.

829 Campbell, J. W. (1995), The lognormal distribution as a model for bio-optical variability in
830 the sea, *J. Geophys. Res.*, 100(C7), 13237-13254.
831 Charria, G., M. Repecaud, L. Quemener, A. Menesguen, P. Rimmelin-Maury, S. L'Helguen,
832 L. Beaumont et al. (2014), PREVIMER: A contribution to in situ coastal observing systems,
833 Mercator Ocean-Quarterly Newsletter, 49, 9-20.
834 Chen, C. T. A., and A. V. Borges (2009), Reconciling opposing views on carbon cycling in
835 the coastal ocean: Continental shelves as sinks and near-shore ecosystems as sources of
836 atmospheric CO_2, *Deep Sea Res. Part II*, 56(8-10), 578-590, doi:10.1016/j.dsr2.2009.01.001.
837 Christensen, O. B., M. Drews, J. H. Christensen, K. Dethloff, K. Ketelsen, I. Hebestadt, and
838 A. Rinke (2006), The HIRHAM Regional Climate Model. Version 5, DMI Technical Report No.
839 06-17. Available at http://www.dmi.dk/dmi/tr06-17.pdf
840 Ciavatta, S., R. Torres, S. Saux-Picart, and J.I. Allen (2011), Can ocean color assimilation
841 improve biogeochemical hindcasts in shelf seas? *J. Geophys. Res.*, 116, C12043.
842 Ciavatta, S., R. Torres, V. Martinez-Vicente, T. Smyth, G. Dall'Olmo, L. Polimene, and J. I.
843 Allen (2014), Assimilation of remotely-sensed optical properties to improve marine
844 biogeochemistry modelling, *Prog. Oceanog.*, 127, 74-95.
845 Cloern, J. E. (2001), Our evolving conceptual model of the coastal eutrophication problem,
846 *Mar. Ecol. Prog. Ser.*, 210, 223-253.
847
848 Daszykowski, M., K. Kaczmarek, Y. Vander Heyden, and B. Walczak (2007), Robust
849 statistics in data analysis—a review: basic concepts, *Chemom. Intell. Lab. Syst.*, 85(2), 203-219.

850 Dee, D. P., S. M. Uppala, A. J. Simmons, P. Berrisford, P. Poli, S. Kobayashi, U. Andrae et
851 al., (2011), The ERA-Interim reanalysis: Configuration and performance of the data assimilation
852 system, *Quart. J. Roy. Meteor. Soc.*, 137(656) 553-597.
853 de Mora, L., M. Butenschön, and J. I. Allen, (2013), How should sparse marine in situ
854 measurements be compared to a continuous model: an example, *Geosci. Model Dev.*, 6(2), 533-
855 548.
856 de Mora, L., M. Butenschön, and J. I. Allen (2016), The assessment of a global marine
857 ecosystem model on the basis of emergent properties and ecosystem function: a case study with
858 ERSEM, *Geosci. Model Dev.*, 9, 59-76, doi:10.5194/gmd-9-59-2016.
859 Diaz, R. J., and R. Rosenberg (2008), Spreading dead zones and consequences for marine
860 ecosystems, *Science*, 321(5891), 926-929.
861 Evensen, G. (1994), Sequential Data Assimilation with a Nonlinear Quasi-Geostrophic Model
862 Using Monte-Carlo Methods to Forecast Error Statistics, *J. Geophys. Res.*, 99(C5), 10143-10162.
863 Evensen, G. (2003), The Ensemble Kalman Filter: theoretical formulation and practical
864 implementation, *Ocean Dynam.*, 53(4), 343-367, doi:10.1007/s10236-003-0036-9.
865 Ferry, N., L. Parent, G. Garric, M. Drevillon, C. Desportes, C. Bricaud, F. Hernandez, (2012),
866 Scientific Validation Report (ScVR) for Reprocessed Analysis and Reanalysis. MyOcean project
867 report, MYO-WP04-ScCV-rea-MERCATOR-V1.0 (No. WP 04 – GLO – MERCATOR).
868 Toulouse, France.
869
870 Fontana, C., C. Grenz, and C. Pinazo (2010), Sequential assimilation of a year-long time-
871 series of SeaWiFS chlorophyll data into a 3D biogeochemical model on the French
872 Mediterranean coast. *Cont. Shelf Res.*, 30(16), 1761-1771.

873 Fontana, C., P. Brasseur, and J. M. Brankart (2013), Toward a multivariate reanalysis of the
874 North Atlantic ocean biogeochemistry during 1998–2006 based on the assimilation of SeaWiFS
875 chlorophyll data, *Ocean Sci.*, 9, 37-56.
876 Ford, D.A., K. P. Edwards, D. Lea, R. M. Barciela, M. J. Martin, and J. Demaria (2012),
877 Assimilating GlobColor ocean color data into a pre-operational physical-biogeochemical model,
878 *Ocean Sci.*, 8, 751–771.
879 Friedrichs, M. A. M., R. R. Hood, and J. D. Wiggert (2006), Ecosystem model complexity
880 versus physical forcing: Quantification of their relative impact with assimilated Arabian Sea
881 data, *Deep Sea Res. Part II*, 53(5-7), 576-600, doi:10.1016/j.dsr2.2006.01.026.
882 Garcia, H. E., R. A. Locarnini, T. P. Boyer, and J. I. Antonov (2006a), World Ocean Atlas
883 2005, Volume 3: Dissolved Oxygen, Apparent Oxygen Utilization, and Oxygen Saturation. S.
884 Levitus, Ed. NOAA Atlas NESDIS 63, U.S. Government Printing Office, Washington, D.C., 342
885 pp. https://www.nodc.noaa.gov/OC5/WOA05/pubwoa05.html.
886 Garcia, H. E., R. A. Locarnini, T. P. Boyer, and J. I. Antonov (2006b), World Ocean Atlas
887 2005, Volume 4: Nutrients (phosphate, nitrate, silicate). S. Levitus, Ed. NOAA Atlas NESDIS
888 64, U.S. Government Printing Office, Washington, D.C., 396 pp.
889 https://www.nodc.noaa.gov/OC5/WOA05/pubwoa05.html
890 Gehlen, M., R. Barciela, L. Bertino, P. Brasseur, M. Butenschön, F. Chai, A. Crise et al.,
891 (2015), Building the capacity for forecasting marine biogeochemistry and ecosystems: recent
892 advances and future developments, *Journal of Operational Oceanography*, 8(1), s168-s187.
893 Geider, R. J., H. L. MacIntyre, and T. M. Kana (1997), Dynamic model of phytoplankton
894 growth and acclimation: Responses of the balanced growth rate and the chlorophyll a: carbon
895 ratio to light, nutrient-limitation and temperature, *Mar. Ecol. Prog. Ser.*, 148(1-3), 187-200.

Gilbert, D., N. N. Rabalais, R. J. Diaz, and J. Zhang, J. (2010), Evidence for greater oxygen decline rates in the coastal ocean than in the open ocean, *Biogeosciences*, 7(7), 2283-2296.

Grant M., T. Jackson T., A. Chuprin, S. Sathyendranath, M. Zuhlke, T. Storm, M. Boettcher, and N. Fomferra (2015), Product user guide, Technical Report D3.4 PUG, Ocean Color Climate Change Initiative (OC_CCI) – Phase Two, European Space Agency, http://www.esa-oceancolor-cci.org

Greenwood, N., E. R. Parker, L. Fernand, D. D. Sivyer, K. Weston, S. J. Painting, S. Kröger, R. M. Forster, H. E. Lees, D. K. Mills, and R.W.P.M Laane (2010), Detection of low bottom water oxygen concentrations in the North Sea; implications for monitoring and assessment of ecosystem health, *Biogeosciences*, 7, 1357-1373, doi:10.5194/bg-7-1357-2010, 2010.

Gregg, W.W. (2008), Assimilation of SeaWiFS ocean chlorophyll data into a three-dimensional global ocean model, *J. Mar. Syst.*, 69, 205-225.

Gregg W. W., and C. S. Rousseaux (2014), Decadal trends in global pelagic ocean chlorophyll: A new assessment integrating multiple satellites, in situ data, and models, *J. Geophys. Res.*, 119(9), 5921-5933.

Gregg, W. W., M. A. M. Friedrichs, A. R. Robinson, K. A. Rose, R. Schlitzer, K. R. Thompson, and S. C. Doney (2009), Skill assessment in ocean biological data assimilation, *J. Mar. Syst.*, 76(1-2), 16-33, doi:10.1016/j.jmarsys.2008.05.006.

Hansell, D. A. (2013), Recalcitrant dissolved organic carbon fractions, *Marine Science*, 5, 421-445, DOI: 10.1146/annurev-marine-120710-100757.

Holt, J. T., and I. D. James (2001), An s coordinate density evolving model of the northwest European continental shelf - 1, Model description and density structure, *J. Geophys. Res.*, 106(C7), 14015-14034.

Holt, J. T., R. Proctor, J. C. Blackford, J. I. Allen, and M. Ashworth (2004), Advective controls on primary production in the stratified western Irish Sea: An eddy-resolving model study, *J. Geophys. Res*., 109, C05024, doi:10.1029/2003jc001951.

Hu, J., K. Fennel, J. P. Mattern, and J. Wilkin (2012), Data assimilation with a local Ensemble Kalman Filter applied to a three-dimensional biological model of the Middle Atlantic Bight, *J. Mar. Syst.*, 94, 145-156.

Hyder, K., A. G. Rossberg, J. I. Allen, M. C. Austen, R. M. Barciela, H. J. Bannister, et al. (2015), Making modelling count-increasing the contribution of shelf-seas community and ecosystem models to policy development and management, *Marine Policy*, 61, 291-302.

Jahnke, (2010), Global Synthesis, in *Carbon and Nutrient Fluxes in Continental Margins: A Global Synthesis* edited by K.-K. Liu, L. Atkinson, R. Quiñones and L. Talaue-McManus, pp. 597-615, IGBP Book Series, Springer, Berlin, Germany,.

James, I. D. (1996), Advection schemes for shelf sea models, *J. Mar. Syst*., 8(3-4), 237-254, doi:10.1016/0924-7963(96)00008-5.

Janjić, T., D. McLaughlin, S. E. Cohn, and M. Verlaan (2014), Conservation of Mass and Preservation of Positivity with Ensemble-Type Kalman Filter Algorithms, *Mon. Weather Rev.*, 142(2).

Jolliff, J. K., J. C. Kindle, I. Shulman, B. Penta, M. A. Friedrichs, R. Helber, and R. A. Arnone, (2009), Summary diagrams for coupled hydrodynamic-ecosystem model skill assessment, *J. Mar. Sys.*, 76(1), 64-82.

Kalman, R. E. (1960), A new approach to linear filtering and prediction problems, *J. Fluids Eng.*, 82(1), 35-45.

941 Kwiatkowski, L., Yool, A., Allen, J. I and other 12 co-authors (2014), iMarNet: an ocean
942 biogeochemistry model intercomparison project within a common physical ocean modelling
943 framework, *Biogeosciences*, 11, 7291-7304, doi:10.5194/bg-11-7291-2014, 2014.
944 Key, R. M., A. Kozyr, C. L. Sabine, K. Lee, R. Wanninkhof, J. L. Bullister, R. A. Feely, F. J.
945 Millero, C. Mordy, and T-H. Peng (2004), A global ocean carbon climatology: Results from
946 Global Data Analysis Project (GLODAP), *Global Biogeochem. Cycles*, 18(4).
947 Kitidis, V., N. J. Hardman-Mountford, E. Litt, I. B., D. Cummings, S. Hartman, D. Hydes et
948 al. (2012), Seasonal dynamics of the carbonate system in the Western English Channel, *Cont.*
949 *Shelf Res.*, 42, 30-40.
950 Lahoz, W. A., and P. Schneider (2014), Data assimilation: making sense of Earth
951 Observation, *Front. Environ. Sci.*, 2, doi: 10.3389/fenvs.2014.00016
952 Lenhart, H. J., D. K. Mills, H. Baretta-Bekker, S. M. Van Leeuwen, J. Van Der Molen, J. W.,
953 J. W. Baretta, et al. (2010), Predicting the consequences of nutrient reduction on the
954 eutrophication status of the North Sea, *J. Mar. Sys.*, 81(1), 148-170.
955 Marrec, P., T. Cariou, E. Macé, P. Morin, L. A. Salt, M. Vernet, B. Taylor, K. Paxman, and
956 Y. Bozec (2015), Dynamics of air–sea CO_2 fluxes in the North-West European Shelf based on
957 Voluntary Observing Ship (VOS) and satellite observations, *Biogeosciences*, 12, 5371-5391.
958 DOI:10.5194/bg-12-5371-2015.
959 Mattern, J. P., M. Dowd, and K. Fennel (2013), Particle filter-based data assimilation for a
960 three-dimensional biological ocean model and satellite observations, *J. Geophys. Res.*, 118(5),
961 2746-2760.Mood, A. M., F. A. Graybill, and D. C. Boes (1974), Introduction to the Theory of
962 Statistics. 3rd ed., McGraw-Hill, New York, USA.

963 Natvik, L. J., and G. Evensen (2003), Assimilation of ocean color data into a biochemical
964 model of the North Atlantic - Part 1. Data assimilation experiments, *J. Mar. Syst.*, 40, 127-153,
965 doi:10.1016/s0924-7963(03)00016-2.
966 Nerger, L., and W. W. Gregg (2007), Assimilation of SeaWiFS data into a global ocean-
967 biogeochemical model using a local SEIK filter, *J. Mar. Syst.*, 68, 237-254,
968 doi:10.1016/j.jmarsys.2006.11.009.
969 O'Boyle, S., and G. Nolan (2010), The Influence of Water Column Stratification on Dissolved
970 Oxygen Levels in Coastal and Shelf Waters Around Ireland, in *Biology and Environment:*
971 *Proceedings of the Royal Irish Academy*, pp. 195-209, Royal Irish Academy, Ireland.
972 OSPAR (2013), Common Procedure for the Identification of the Eutrophication Status of the
973 OSPAR Maritime Area, Technical Report, Reference number: 2013-8,
974 www.ospar.org/documents?d=32957
975 Patsch, J., H. J. Lenhart (2004), Daily loads of nutrients, total alkalinity, dissolved inorganic
976 carbon and dissolved organic carbon of the European continental rivers for the years 1977-2002,
977 Issue 48 of Berichte aus dem Zentrum für Meeres- und Klimaforschung / B: Ozeanographie /
978 Institut für Meereskunde, Zentrum für Meeres- und Klimaforschung,
979 www.ifm.zmaw.de/fileadmin/files/theoretical_oceanography/Modelldaten_JP/RIVER.pdf
980 Pauly, D., V. Christensen, S. Guénette, T. J. Pitcher, U. R. Sumaila, C. J. Walters, R. Watson,
981 and D. Zeller (2002), Towards sustainability in world fisheries, *Nature*, 418, 689-695.
982 Pinna, A., L. Pezzolesi, R. Pistocchi, S. Vanucci, S. Ciavatta, L. Polimene (2015), Modelling
983 the Stoichiometric Regulation of C-Rich Toxins in Marine Dinoflagellates, *PloS one*, 10(9),
984 e0139046.

985 Piroddi, C., H. Teixeira, C. P. Lynam, C. Smith, M. C. Alvarez, K. Mazik, E. Andonegi et al.
986 (2015), Using ecological models to assess ecosystem status in support of the European Marine
987 Strategy Framework Directive, *Ecol. Indic.*, 58, 175-191.
988 Polimene, L., J. I. Allen, and M. Zavatarelli (2006), Model of interactions between dissolved
989 organic carbon and bacteria in marine systems, *Aquat. Microb. Ecol.*, 43(2), 127-138.
990 Rabalais, N. N., W.-J. Cai, J. Carstensen, D. J. Conley, B. Fry, X. Hu, Z. Quinones-Rivera et
991 al. (2014), Eutrophication-driven deoxygenation in the coastal ocean, *Oceanography*, 27(1), 172-
992 183.
993 Rousseaux, C. S., and W. W. Gregg (2015), Recent decadal trends in global phytoplankton
994 composition, *Global Biogeochem. Cycles*, 29, 1674–1688, doi:10.1002/2015GB005139.
995 Sathyendranath, S. (2000). Reports of the International Ocean-Color Coordinating Group.
996 IOCCG, Dartmouth, Canada, 3, 140.
997 Sathyendranath, S., and T. Jackson (2015), Comprehensive Error Characterization Report,
998 Technical Report CECR, , Ocean Color Climate Change Initiative (OC_CCI) – Phase Two,
999 European Space Agency, http://www.esa-oceancolor-cci.org.
1000 Sathyendranath, S., R. J. W. Brewin, C Brockman and other 37 co-authors, Creating an
1001 ocean-colour time series for use in climate studies: the experience of the ocean-colour climate
1002 change initiative, *Remote Sens. Environ.*, submitted.
1003 Saux Picart, S., M. Butenschön, and J. D. Shutler (2012), Wavelet-based spatial comparison
1004 technique for analysing and evaluating two-dimensional geophysical model fields, *Geosci.*
1005 *Model Dev.*, 5(1), 223-230.

1006 Shulman, I., Frolov, S., Anderson, S., Penta, B., Gould, R., Sakalaukus, P., Ladner, S., 2013.
1007 Impact of bio-optical data assimilation on short-term coupled physical, bio-optical model
1008 predictions. *J. Geophys. Res.*, 118(4), 2215-2230.
1009 Simon, E., and L. Bertino (2009), Application of the Gaussian anamorphosis to assimilation
1010 in a 3-D coupled physical-ecosystem model of the North Atlantic with the EnKF: a twin
1011 experiment, *Ocean Sci.*, 5(4), 495-510.
1012 Skogen, M. D., K. Eilola, J. L. Hansen, H. M. Meier, M. S. Molchanov, and V. A.
1013 Ryabchenko (2014), Eutrophication status of the North Sea, Skagerrak, Kattegat and the Baltic
1014 Sea in present and future climates: A model study. *J. Mar. Sys.*, 132, 174-184.
1015 Stockdale, T. N., D. L. T. Anderson, J. O. S. Alves, and M. A. Balmaseda (1998), Global
1016 seasonal rainfall forecasts using a coupled ocean atmosphere model, *Nature*, 392, 370–373. doi:
1017 10.1038/32861.
1018 Storto, A, S. Masina, and S. Dobricic (2013), Ensemble spread-based assessment of
1019 observation impact: application to a global ocean analysis system, *Quart. J. Roy. Meteor. Soc.*,
1020 139(676), 1842-1862.
1021 Taylor, K. E. (2001), Summarizing multiple aspects of model performance in a single
1022 diagram, *J. Geophys. Res.*, 106(D7), 7183-7192.
1023 Teruzzi, A., S. Dobricic, C. Solidoro, and G. Cossarini (2014), A 3-D variational assimilation
1024 scheme in coupled transport-biogeochemical models: Forecast of Mediterranean biogeochemical
1025 properties, *J. Geophys. Res.*, 119, 200–217.
1026 Thomas, H., Y. Bozec, H. J. W. De Baar, K. Elkalay, M. Frankignoulle, L-S. Schiettecatte, G.
1027 Kattner, and A. V. Borges (2005), The carbon budget of the North Sea, *Biogeosciences*, 2(1), 87-
1028 96.

1029 Torres, R., J. I. Allen, and F. G. Figueiras (2006), Sequential data assimilation in an upwelling
1030 influenced estuary, *J. Mar. Syst.*, 60(3-4), 317-329, doi:10.1016/j.jmarsys.2006.02.001.
1031 Tørseth, K., W. Aas, K. Breivik, A. M. Fjæraa, M. Fiebig, A. G. Hjellbrekke, C. Lund Myhre,
1032 S. Solberg, and K. E. Yttri. (2012), Introduction to the European Monitoring and Evaluation
1033 Programme (EMEP) and observed atmospheric composition change during 1972–2009, *Atmos.*
1034 *Chem. Phys.*, 12(12), 5447-5481.
1035 Trenberth, K. E., and J. G. Olson (1988), An evaluation and intercomparison of global
1036 analyses from NMC and ECMWF*, Bull. Am. Meteorol. Soc*., 69, 1047–1057.
1037 Triantafyllou, G., G. Korres, I. Hoteit, G. Petihakis, and A. C. Banks (2007), Assimilation of
1038 ocean color data into a biogeochemical flux model of the eastern Mediterranean Sea, *Ocean Sci.*,
1039 3, 397-410.
1040 Vaquer-Sunyer, R., and C. M. Duarte (2008), Thresholds of hypoxia for marine biodiversity,
1041 *PNAS*, 105(40), 15452-15457.
1042 Vörösmarty, C.J., B. Fekete, and B.A. Tucker (1996), River Discharge Database, Version 1.0
1043 (RivDIS v1.0), Volumes 0 through 6. A contribution to IHP-V Theme 1. Technical Documents
1044 in Hydrology Series. UNESCO, Paris.
1045 Wakelin, S. L., J. T. Holt, J. Blackford, J. I. Allen, M. Butenschön, and Y. Artioli (2012),
1046 Modeling the carbon fluxes of the northwest European continental shelf: Validation and budgets,
1047 *J. Geophys. Res.*, 117(C5).
1048 While, J., I. Totterdell, and M. Martin (2012), Assimilation of pCO_2 data into a global
1049 coupled physical-biogeochemical ocean model, *J. Geophys. Res.*, 117(C3).

1050 Xiao, Y., and M.A.M. Friedrichs (2014), Using biogeochemical data assimilation to assess the
1051 relative skill of multiple ecosystem models: effects of increasing the complexity of the
1052 planktonic food web, *Biogeosciences*, 11(11), 3015-3030.